

Impact of Industrial Constraints on the Dynamic Performance of a PID-Controlled Hybrid Heat-Integrated Distillation System with a Plate Heat and Mass Exchanger

Mariusz Markowski¹, Marian Trafczynski^{1*}, Erika Pavlovičová², Juraj Oravec²,
Slawomir Alabrudzinski¹, Piotr Kisielewski¹, Krzysztof Urbaniec¹, Kacper Elwertowski¹,
Damian Gostynski¹

¹ Faculty of Civil Engineering Mechanics and Petrochemistry, Institute of Mechanical Engineering, Warsaw
University of Technology, Lukasiewicza 17, 09-400 Plock, Poland
e-mail: marian.trafczynski@pw.edu.pl

² Faculty of Chemical and Food Technology, Institute of Information Engineering, Automation, and
Mathematics, Slovak University of Technology in Bratislava, Radlinského 9, 812-37 Bratislava, Slovakia
e-mail: juraj.oravec@stuba.sk

Abstract

A dynamic model for the Hybrid Heat-Integrated Distillation System (HHIDiS) incorporating a Heat and Mass Exchanger (HME) was developed. The system's behaviour under PID control was simulated using Simulink/MATLAB, with a focus on examining the effects of industrial constraints, such as fouling growth on heat exchanger surfaces and liquid hold up within the plate HME on operational quality indices. Results revealed that increases in fouling resistance or liquid hold up alter the thermal inertia of the HME, condenser, and reboiler, subsequently impacting the dynamic performance of PID control loops. These effects were analysed by simulating the closed-loop HHIDiS system at varying stages of fouling accumulation and liquid retention. Changes caused by fouling and liquid hold up were reflected in control quality indices such as overshoot, peak time, delay time, rise time, and settling time. Such variations may compromise PID control effectiveness. The findings emphasise the need to adjust PID tuning parameters to maintain optimal control performance when industrial constraints shift. Adverse effects can be mitigated through periodic recalibration of PID gains. Simulation results demonstrated that the proposed HHIDiS system remains dynamically stable despite these challenges and that standard PID controllers are suitable for its operation. These insights highlight the importance of proactive control adjustments to sustain high performance under evolving industrial conditions.

Keywords

Heat-integrated distillation; Heat and mass exchanger; Hybrid system; Thermal separation; Dynamic model; Lumped-parameter approach; Control quality.

Highlights

A PID-controlled HHIDiS system is dynamically modelled using Simulink/MATLAB. Industrial constraints, including fouling and liquid hold up, affect thermal inertia and control. Fouling and hold up of liquid alter dynamic responses and degrade PID control performance. Periodic PID tuning mitigates adverse effects and ensures control quality under constraints. HHIDiS remains dynamically stable, with PID controllers suitable for industrial applications.

1. Introduction

* Corresponding author

Distillation is a fundamental operation in industrial processes, particularly in the fields of petroleum refining, petrochemicals, and other large-scale chemical industries. This separation technique is among these sectors' most energy-intensive unit operations [1]. According to work [2], approximately 45% of the total energy consumed within the petroleum and chemical industries can be traced to distillation processes [3]. This substantial energy usage also entails significant resource consumption, including water, coal, and natural gas. These inefficiencies lead to extensive energy losses, accumulating over time and creating a considerable environmental impact. To address these issues, the concept of heat-integrated distillation technology has emerged as a groundbreaking and energy-saving method. Properly designed and implemented heat-integrated distillation column (HIDiC) systems can significantly reduce energy consumption compared to conventional distillation columns. This energy-saving potential underscores the importance of advancing the modeling and control systems of HIDiC processes, particularly as industries strive to lower their carbon footprints and meet global environmental goals [4].

The role of distillation extends far beyond a single industry. Globally, distillation columns are responsible for approximately 95% of all industrial separation processes, making them indispensable for manufacturing and chemical production. However, this widespread application comes with a hefty energy demand, accounting for roughly 3% of the total global energy consumption. Such a figure highlights the urgency of optimising distillation technologies to mitigate their environmental and economic impacts. The application of HIDiC technology offers an opportunity to address these energy concerns on a global scale. By reducing the heat consumption of distillation systems by 40% to 60% compared to traditional industrial solutions [5], HIDiC technology could potentially lower global energy consumption by 1.5%. The significance of these advancements is clear when considering the broader context of energy sustainability. Traditional distillation systems are inherently energy-intensive due to the high thermal requirements needed to separate components based on their boiling points. These systems often operate inefficiently, losing significant amounts of energy through heat dissipation and other inefficiencies. HIDiC technology addresses this by integrating advanced heat recovery mechanisms, which recycle energy within the system and drastically reduce the external energy input required for operation. However, implementing HIDiC technology does come with its own challenges. Designing and optimising these systems require sophisticated modeling and control strategies to ensure stable and efficient operation. Retrofitting existing distillation units with heat integration features can be complex and costly; nevertheless, the potential benefits far outweigh these challenges, as adopting HIDiC can lead to substantial cost savings, reduced energy demand, and lower greenhouse gas emissions over the long term.

Industrial separation processes commonly rely on a distillation column, supported by essential auxiliary equipment such as a condenser and a reboiler (see Fig. 1a). While this conventional system is widely used, it is known for its significant energy demands. The reboiler requires substantial heat input (\dot{Q}_R), and the condenser experiences considerable heat loss (\dot{Q}_C). Due to the inefficiencies associated with these systems, researchers have focused on developing energy-saving alternatives, with HIDiCs being a prominent area of study. Comprehensive reviews by researchers like Jana [1] and Fang et al. [6] offer an in-depth analysis of the advancements in HIDiC technology. The HIDiC system introduces a transformative approach to traditional distillation by incorporating a compressor that creates a pressure differential between the rectifying and stripping sections. This design innovation facilitates heat recovery from the rectifying section to the stripping section via thermal coupling across the wall (illustrated in Fig. 1b). By separating the distillation column into distinct rectifying and stripping sections, the system allows for temperature regulation across these zones. A compressor elevates the pressure and temperature in the rectifying section, enabling heat transfer to the lower-temperature stripping section. Consequently, this design significantly

reduces the condenser and reboiler's energy load. Despite the additional energy consumption required by the compressor, the overall energy efficiency is greatly improved due to the enhanced internal heat recovery.

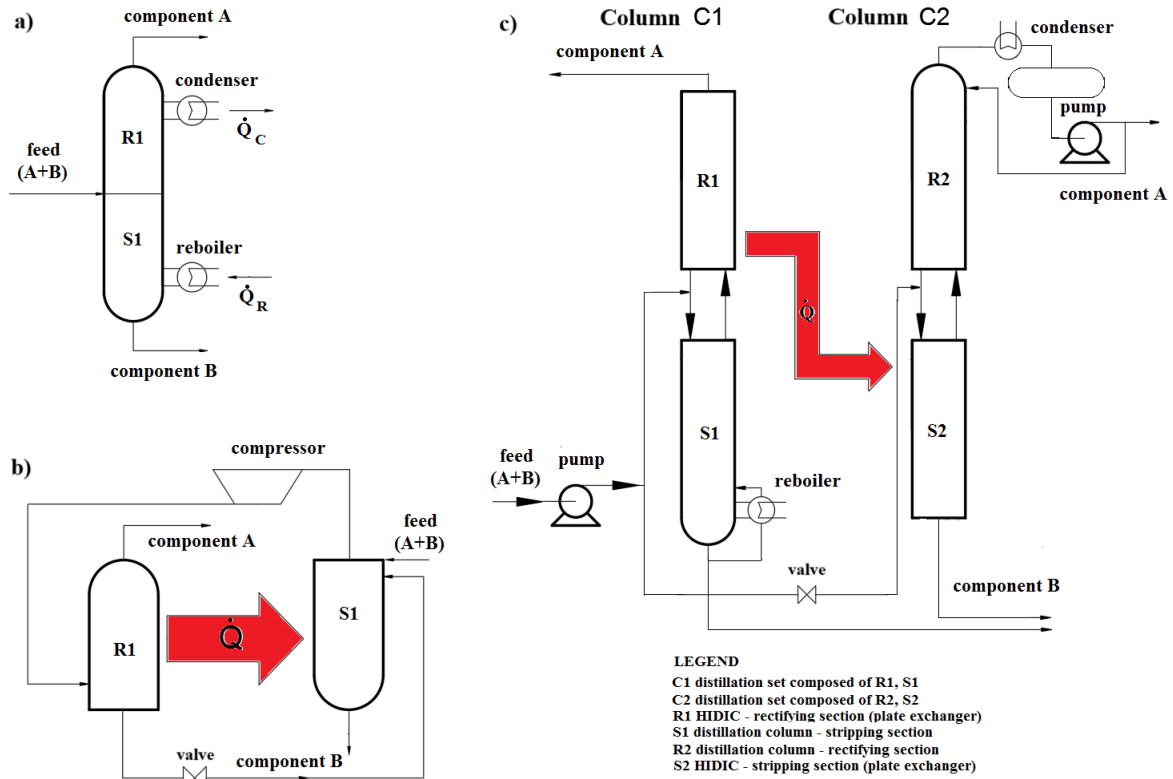


Figure 1. Schematic diagram of: a) industrial distillation column, b) HIDiC, c) HHIDiS.

Markowski et al. [5] further expanded upon this concept by introducing a mathematical model for a hybrid heat-integrated distillation system (HHIDiS), as depicted in Fig. 1c. In this configuration, the distillation system consists of two specialised sections: one for heat integration (R1 and S2) and another for maintaining stability during dynamic operations (S1 and R2). The integration of R1 and S2 employs plate or channel Z-type heat and mass exchangers (HME) [7], which are thermally linked to the stripping (S1) and rectifying (R2) sections of traditional distillation columns. This thermal coupling facilitates more effective heat recovery, reducing energy requirements by integrating heat between the R1 and S2 sections. Moreover, the dynamic stabilisation achieved by the S1 and R2 sections enhances the overall operational reliability of the system. Unlike conventional HIDiCs that rely on a compressor to regulate the pressure difference (Fig. 1b), the system proposed by Markowski et al. [5] adjusts the pressure differential between R1 and S2 using a pump and a valve (Fig. 1c). This alternative approach offers notable advantages, including reduced susceptibility to mechanical failures and lower capital investment costs. Preliminary findings indicate that this novel configuration can achieve approximately a 10% reduction in energy consumption compared to traditional systems. To extend the applicability of this innovative design, the authors integrate the R1 and S2 sections within two separate columns (C1 and C2), as shown in Fig. 1c. This approach contrasts with most existing HIDiC solutions, which typically thermally integrate the rectifying and stripping sections within a single column (Fig. 1b). By introducing this dual-column design, the new system improves operational flexibility and further optimises energy utilisation.

The concept of HIDiCs has been widely explored in the literature, with numerous variations and configurations proposed. Different geometries have been investigated to optimise heat exchange efficiency. For instance, one commonly studied design involves a concentric configuration where the rectifying section is positioned inside an annular stripping section, as discussed in [8]. Harvindran and Foo [9] provided a comprehensive overview of HIDiC technology and outlined a systematic approach to the design of HIDiC systems. Meanwhile, Kiss and Olujić [10] and Fang et al. [6] reviewed the advancements and challenges associated with HIDiC processes. In terms of optimisation, Velázquez et al. [11] introduced a hybrid strategy aimed at improving HIDiC design performance. The authors proposed an optimisation method combining deterministic Mixed-Integer Nonlinear Programming (MILP) to determine optimal heat integration points and stochastic simulated annealing for faster optimisation. These findings underline the promise of advanced modeling and optimisation techniques in enhancing HIDiC performance and control. Marin-Gallego et al. [12] contributed to this research by developing novel column packing specifically tailored for HIDiCs, enhancing the balance between heat and mass transfer efficiency. However, not all studies highlight consistent benefits. For example, Kagioulis et al. [13] examined the application of HIDiC to an ethylene fractionator and observed that, while utility demands for the distillation column were reduced, overall process utility consumption increased slightly. Other researchers, Harwardt and Marquardt [14] and Shenvi et al. [15], suggest that heat pump systems with limited heat transfer points outperform HIDiCs with continuous heat integration. Additionally, HIDiC technology has been extended to reactive distillation processes, as presented by Eyvazi-Abhari et al. [16] and Gao et al. [17]. Also, significant work has been conducted on control strategies for HIDiC operations, introduced by Cong et al. [4], Gutiérrez-Guerra et al. [18], and Liu et al. [19]. The nonlinear nature of the HIDiC presents notable difficulties for online operation. Addressing these difficulties necessitates the use of precise nonlinear models for optimisation or control system design [4]. Nonetheless, the thermal interactions between the rectifying and stripping sections introduce intricate dynamic behaviour and pronounced nonlinearity, complicating online control efforts [10,20]. Traditional PID control and methods relying on linear approximation models typically demand considerable fine-tuning and are constrained by narrow operational ranges. Consequently, designing control systems based on nonlinear models is critically important [21-23]. Ho et al. [24] developed a modular simulator for dynamic distillation that integrates variable pressure across rectifying trays; dynamic vapour hold up, and energy balance. They also considered the effect of pressure on product purity and implemented equations to model the system's response to pressure changes, showing that internally, HIDiCs can achieve dynamic parameters similar to traditional distillation columns. This suggests that HIDiC control in industrial applications is technically feasible. Seo et al. [25] studied internal HIDiC configurations, achieving lower internal flow rates and energy use compared to direct sequences and Reactive Dividing Wall Columns (RDWCs), with utility reductions of 15.4% and 14.4%, respectively, through a partial double annular structure. Huang et al. [26] explored HIDiC dynamics, proposing control configurations to minimise energy consumption [27]. Similarly, [28] used mass and energy balance equations, assuming liquid-vapor thermodynamic equilibrium, to model HIDiC dynamics, revealing significant input-output nonlinearity, such as gain variability under different conditions. For instance, Jana [29] introduced a batch HIDiC configuration using vapour recompression (VRC) with heat pumps, reducing energy consumption, CO₂ emissions, and costs. Nakaiwa et al. [30] proposed feedback control configurations for HIDiC, identifying distillate and residue liquid reflux as optimal for control. Research on HIDiC modeling, design, and control highlights efforts to improve efficiency and sustainability. In a recent paper [31], Gutiérrez-Guerra and Segovia-Hernández presented a new method for designing and optimising HIDiC columns with a stochastic optimisation algorithm and Aspen Plus. This method was created to address convergence issues

to maintain a continuous optimisation process while improving the search for the best solutions. The method's effectiveness was demonstrated by the HIDIc columns' optimisation during the separation of four close-boiling binary mixtures. According to the results, the strategy used proved effective in addressing these columns' design and optimisation. Consequently, the method made it possible to lessen convergence issues, maintain an ongoing optimisation process, and enhance the calibre of the solutions that were discovered. The Authors stated that based on this approach, other binary HIDIc columns can be designed and optimised using an approximated short-cut method. On the other hand, this strategy could be expanded to design and optimise HIDIc columns for ternary mixture separation with the right modification. Gutiérrez-Guerra et al. [18] presented the dynamic performance of HIDIcs. The dynamic performance was evaluated for the previously optimised HIDIc designs using a constrained Boltzmann-based distribution estimation algorithm. Eight close-boiling mixtures with varying relative volatile contents were employed as case studies. The dynamic behaviour was identified through process analysis in closed and open loops. The outcomes demonstrated that, across all case studies, the HIDIc columns perform less dynamically than their traditional equivalents. It was also well-known that, for the majority of systems, the disparity between the two configurations' dynamic behaviours maintained a comparatively consistent trend. However, an important difference in the dynamic characteristics was identified for the mixture nearing azeotropic behaviour, requiring a significantly greater degree of control. Gutiérrez-Guerra and Segovia-Hernández [32] investigated how control properties influence the energy-efficient and cost-effective operation of HIDIcs under varying feed compositions. Using the Integral Absolute Error (IAE) criterion and detailed simulations performed in Aspen Dynamics, they assessed the control properties through closed-loop process evaluations. Their findings revealed that HIDIc configurations offering optimal energy and economic performance differed from those with the most favorable dynamic behavior. However, HIDIc setups with suboptimal configurations demonstrated superior dynamic characteristics while only slightly compromising energy efficiency and cost-effectiveness.

1.1. The novelty of the work

This paper aims to provide several contributions to the understanding and application of the HHIDIS system. First, the authors developed a comprehensive dynamic model of the entire HHIDIS system, which is depicted schematically in Fig. 1c. This effort builds on their previous work, which presented a dynamic model of the plate HME (sections R1-S2), as outlined in reference [33]. The new contributions include dynamic models for additional system components: the reboiler, condenser, rectification section R2 of distillation column C2, and stripping section S1 of distillation column C1. These new models are developed using a lumped-parameters approach to mathematical modelling that draws from widely recognised methods for heat exchangers and distillation columns detailed in the literature. The majority of HIDIc configurations discussed in existing literature, such as those featuring compressors (as shown in Figure 1b), are dynamically controllable technologies. These studies often explore the relationship between dynamic behaviour and the optimisation of energy and economic performance for various close-boiling binary mixtures and fluctuating feed compositions. However, in contrast, this study focuses on a novel configuration. The dynamic behavior of a PID-controlled HHIDIS system without a compressor (illustrated in Fig. 2) is analysed under realistic industrial constraints. Specific considerations include the accumulation of fouling on heat transfer surfaces and the hold up of liquid within the plate HME exchanger. To understand these effects, simulations were conducted on both open- and closed-loop systems under varying stages of these constraints. The evaluation of the influence of fouling and liquid hold up considered key control performance indices, including overshoot, peak time, delay time, rise time, and settling time.

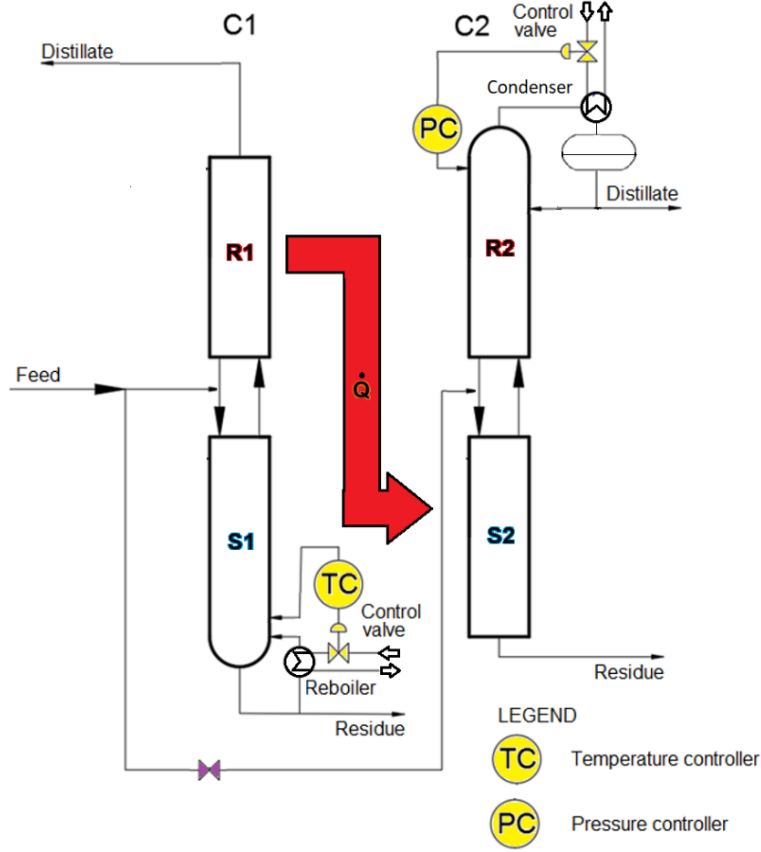


Figure 2. Scheme of a process control system for the HHIDiS (symbols according to Fig. 1c).

To the best of the authors' knowledge, this analysis represents a novel contribution to the study of HIDiC systems. Existing research typically emphasises idealised process conditions in dynamic and steady-state HIDiC models. However, these studies often overlook the industrial constraints that would likely impact HIDiC technology in real-world applications. This work seeks to address that gap by focusing on the potential future application of HIDiC technology within industrial environments. The case study highlights the importance of considering the dynamic properties of the HHIDiS system, along with its proposed PID control methodology, during the early stages of research and development. This proactive approach, ideally implemented during the design and prototyping phases, facilitates the cost-effective design of process equipment while preemptively addressing challenges related to control systems. Failure to incorporate the dynamic characteristics of the process during the design phase could necessitate the development of complex and expensive control systems, which would significantly increase operational costs. By addressing these considerations early on, the research contributes to advancing the practical viability of HHIDiS systems in industrial applications.

2. Dynamic models of the HHIDiS system

Optimising HHIDiS performance under evolving conditions, such as fouling over time, requires adopting dynamic models tailored to the situation. These models can use distributed or lumped parameters, each offering distinct benefits and limitations that define their suitability for specific scenarios. A detailed evaluation of these modelling methods is presented in reference [34]. Section 2 discusses dynamic models for the HHIDiS system, featuring two PID control loops that manage temperature and pressure, as illustrated in Fig. 2. Subsequent sections

highlight both established and novel models introduced in this research, including dynamic representations of the plate HME, reboiler, condenser, stripping section S1 of column C1, and rectification section R2 of column C2.

2.1. The dynamic model of plate HME

The mathematical model of plate HME in the steady state was taken from the study by Markowski et al. [5] and in the dynamic state – by Markowski et al. [33]. The authors proposed a Z-type plate HME [35] for simultaneous diaphragm heat exchange and distillation processes – Fig 3c, and decided to explore this solution because it requires less capital outlay than other types, such as shell-and-tube heat exchangers. Fig. 3a illustrates the concept of thermal coupling R1 and S2 sections, which is widely recognised in the literature.

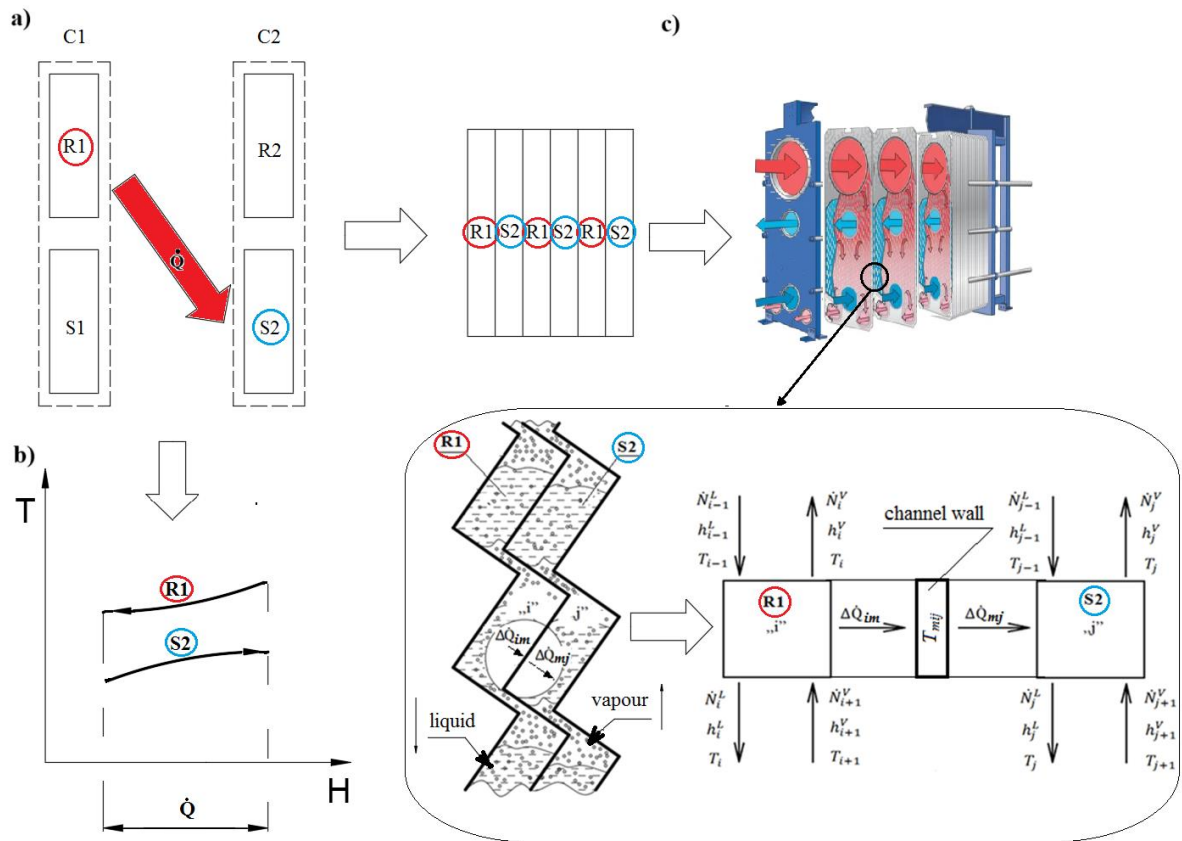


Figure 3. The concept involves reconfiguring the rectifying section R1 of column C1 and the stripping section S2 of column C2 into a plate HME. This includes: a) the idea of heat integration between R1 and S2, b) column profiles T–H, and c) an HME constructed from channels using a Z-type plate exchanger [35] divided into cells „i” and „j” used for mass and energy balances.

The mathematical description for the steady-state HME system integrates two distinct approaches: the Diaphragm Heat Exchange Model (formulated using principles from thermal resistance theory) and the Mass Transfer Model (grounded in the theoretical tray concept commonly applied to distillation processes). The diaphragm heat exchange process is quantified using standard equations that are widely employed in heat exchanger calculations and referenced in [5]. The temperature difference ΔT is determined by analysing the column profiles of the rectifying section R1 and the stripping section S2. The heat integration mechanism between these two sections, along with their respective T–H column profiles, is illustrated in Fig. 3ab. Commonly used equations in the calculations of the distillation column describe the

mass transfer phenomena, employing the concept of the theoretical tray [5]. A set of cells addressed using the lumped-parameter technique comprised the channel-type exchanger model (Fig. 3c). Differential equations from the mass and energy balances were used to characterise each cell. Additionally, each cell was placed in an area with intensive vapour-liquid mixing. Subsequently, the theoretical tray was assumed to correspond to the mixing zone. The energy and mass balances for the i -th and j -th mixing regions in plate HME, representing an equivalent theoretical tray (refer to Fig. 3c), are extensively described in the previous authors' work [33]. The formulated there [33] energy balance for steady-state conditions can describe a dynamic state by accounting for heat accumulation in „ i ” and „ j ” cells – see Fig 3c. Specifically:

$$\frac{d(N_j \cdot h_j^L)}{dt} = \dot{N}_{j-1}^L \cdot h_{j-1}^L + \dot{N}_{j+1}^V \cdot h_{j+1}^V + \Delta\dot{Q}_{mj} - \dot{N}_j^V \cdot h_j^V - \dot{N}_j^L \cdot h_j^L \quad (1)$$

$$\frac{d(N_i \cdot h_i^L)}{dt} = \dot{N}_{i-1}^L \cdot h_{i-1}^L + \dot{N}_{i+1}^V \cdot h_{i+1}^V - \dot{N}_i^L \cdot h_i^L - \dot{N}_i^V \cdot h_i^V - \Delta\dot{Q}_{im} \quad (2)$$

The energy balance for the cell wall is described by:

$$\rho_m \cdot V_m \cdot c_m \cdot \frac{dT_m}{dt} = -\Delta\dot{Q}_{mj} + \Delta\dot{Q}_{im} \quad (3)$$

The heat transfer within the i,j cell, assuming no fouling effects, is expressed as:

$$\Delta\dot{Q}_{im} = h_c \cdot (T_i - T_{mij}) \cdot \Delta A_{i,j} \quad (4)$$

$$\Delta\dot{Q}_{mj} = h_b \cdot (T_{mij} - T_j) \cdot \Delta A_{i,j} \quad (5)$$

The mass balance for „ i ” and „ j ” cells is represented by the following equations:

$$\frac{dN_i^L}{dt} = \dot{N}_{i-1}^L - \dot{N}_i^L + \frac{\Delta\dot{Q}_{im}}{B_i} \quad (6)$$

$$\frac{dN_j^L}{dt} = \dot{N}_{j-1}^L - \dot{N}_j^L - \frac{\Delta\dot{Q}_{mj}}{B_j} \quad (7)$$

$$\frac{dN_i^V}{dt} = \dot{N}_{i+1}^V - \dot{N}_i^V - \frac{\Delta\dot{Q}_{im}}{B_i} \quad (8)$$

$$\frac{dN_j^V}{dt} = \dot{N}_{j-1}^V - \dot{N}_j^V + \frac{\Delta\dot{Q}_{mj}}{B_j} \quad (9)$$

The mathematical model assumes thermodynamic equilibrium between the vapour and liquid phases; the steady-state mass balance is also a fundamental assumption. Initially, equations (4)-(5) and (6)-(9) were incorporated into the energy balance equations, Eqs. (1)-(3). These combined equations were then linearised and subjected to a Laplace transformation for further analysis.

The operator transmittances for ten individual cells were interconnected through signal pathways, establishing a comprehensive relationship among them. A block diagram representing this interconnected system illustrates the dynamic structure and behaviour of the tested HME model. The block diagram shown in Fig. 4 provides a visual framework for understanding the interaction of transmittances across the system's various components. Based

on the distinct signals of the variables coming into and going out of the apparatus, the HME dynamic model [33] was constructed. Fig. 4 displays the model of two nearby cells, "i" and "j". Block no. 1 in Fig. 4, which represents the transmittances from G_1 to G_{16} , constitutes the first interaction associated with energy exchange. The transfer functions from G_{17} to G_{28} (block no. 2 in Fig. 4) illustrate the mass exchange. Lastly, the impact of pressure on the apparatus dynamics - transmittances from G_{29} to G_{32} in block 3 of Fig. 4 - was considered. A cell's output signals are input signals by cells following it.

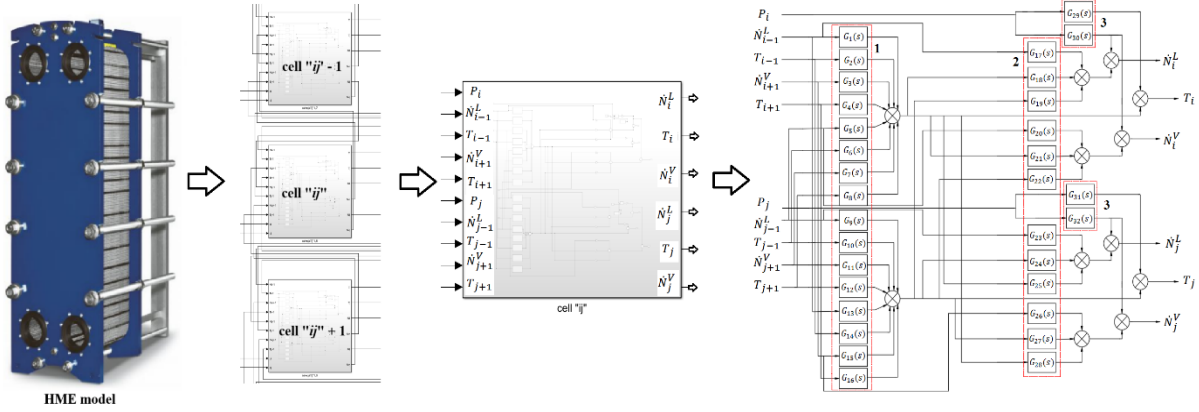


Figure 4. Block diagram details for the "i, j" cell of the HME dynamic model [33].

2.2. The dynamic models of rectification R2 and stripping S1 sections of the distillation columns

Subsection 2.2. presents the developed dynamic models of the stripping section S1 and the rectification section R2 of classical distillation columns C1 and C2, respectively, as schematically shown in Figure 2.

The energy balance of a control volume is used to create the equation that characterises the dynamic behaviour of the rectifying R2 section (see Fig. 5a, where the control volume is considered to be the whole rectifying R2 section volume in column C2 – lumped parameter model).

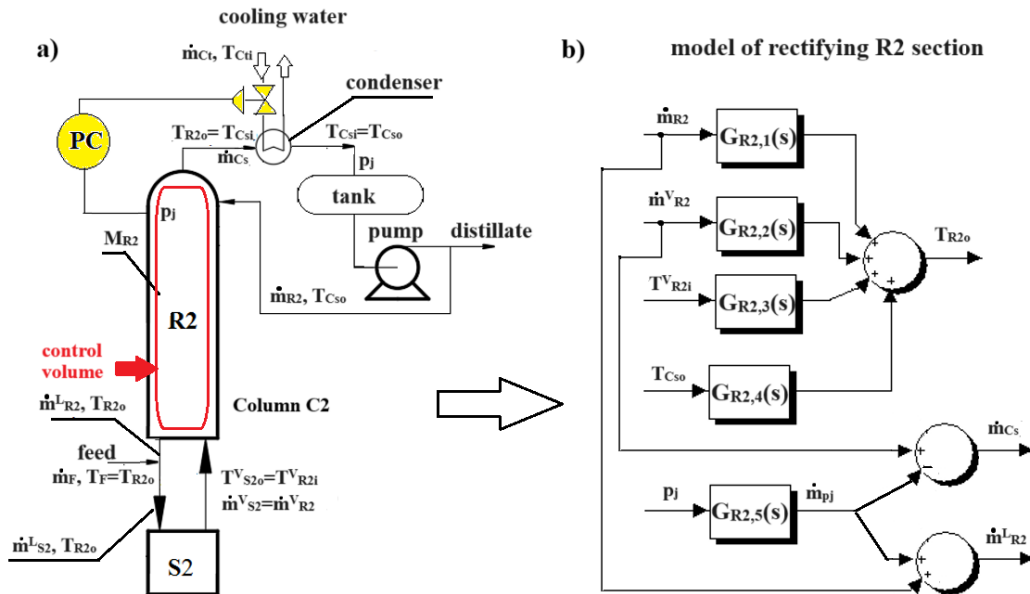


Figure 5. The scheme of distillation column C2 – a), and the block diagram for the dynamic model of the rectifying R2 section – b).

The energy accumulation within the control volume is determined by the difference between the energy carried by the incoming fluid and the energy carried away by the outgoing fluid:

$$M_{R2} \cdot c_{R2o} \cdot \frac{dT_{R2o}}{dt} = \dot{m}_{R2}^V \cdot (c_{R2i}^V \cdot T_{R2i}^V + r_{R2i}^V) + \dot{m}_{R2} \cdot c_{R2}^L \cdot T_{Cso} - \dot{m}_{R2}^L \cdot c_{R2o}^L \cdot T_{R2o} - \dot{m}_{Cs} \cdot (c_{R2o}^V \cdot T_{R2o} + r_{R2o}^V) \quad (10)$$

The dynamic model of the rectifying R2 section for distillation column C2 was constructed by isolating the signals corresponding to variables entering and exiting the apparatus, as depicted in Fig. 5b. Initially, the interactions associated with energy transfer, as defined by Eq. (10), were analysed to determine the transmittances ranging from $G_{R2,1}$ to $G_{R2,4}$. Additionally, the model incorporated the effects of pressure on the apparatus's dynamic behaviour, represented by the transmittance $G_{R2,5}$.

The equation that characterises the dynamic behaviour of the stripping section, S1, is developed based on the energy balance within a defined control volume. As depicted in Fig. 6a, the control volume encompasses the entire S1 stripping section within column C1, modelled using a lumped parameter approach. The energy balance assumes that the energy accumulated in the control volume is equivalent to the difference between the energy brought in by the inflowing fluid and the energy removed by the outflowing fluid, according to Eq. (11). The framework so created facilitates understanding the thermodynamic dynamics of the stripping section and its role in the overall column operation.

$$M_{S1} \cdot c_{S1o} \cdot \frac{dT_{S1o}}{dt} = \dot{m}_{S1}^L \cdot c_{S1}^L \cdot T_{R1o}^L + \dot{m}_{Rt} \cdot (c_{Rto} \cdot T_{Rto} + r_{Rto}) - \dot{m}_{S1}^V \cdot (c_{S1o}^V \cdot T_{S1o} + r_{S1o}^V) - \dot{m}_{S1o}^L \cdot c_{S1o}^L \cdot T_{S1o} \quad (11)$$

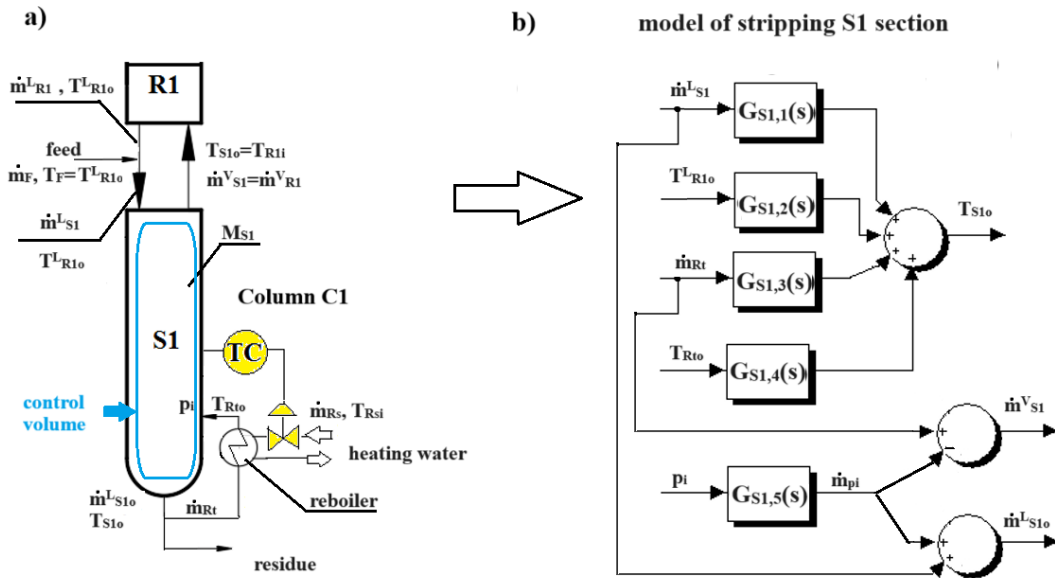


Figure 6. The scheme of distillation column C1 – a), and the block diagram for the dynamic model of the stripping S1 section – b).

The dynamic model of the stripping S1 section for distillation column C1 was developed by isolating the signals corresponding to the variables entering and exiting the apparatus, as depicted in Fig. 6b. Initial analyses focused on energy exchange interactions, described by Eq. (11), which define the transmittances ranging from $G_{S1,1}$ to $G_{S1,4}$. Furthermore, the effect of

pressure on the apparatus's dynamic behaviour was incorporated into the model through the transmittance $G_{S1.5}$. This comprehensive approach ensures that the model accurately captures the system's dynamic characteristics.

2.3. The dynamic models of the condenser and reboiler operating with the distillation columns

The transient behaviour of shell-and-tube heat exchangers, such as condensers and reboilers, can be effectively modelled using a lumped-parameter model with a cell-based approach. Lumped dynamic models have been widely used in dynamic analyses, demonstrating strong correlation with experimental data in several studies [34, 36, 37]. These models are built on the concept of multi-cell topologies, such as mixed tanks [38], where hot and cold cells are interconnected by a wall element that spans the entire length of the heat exchanger. This structure allows representing the heat exchanger as a series of perfectly mixed tanks, each containing hot, cold, and wall-side components. To calculate the system's initial conditions, a steady-state simulation is necessary, during which the temperature across each element remains constant, resulting in constant physical properties throughout. Additionally, the total volume and surface area of the heat exchanger are evenly distributed across the cells, with negligible heat loss to the surroundings. One of the main benefits of using a cell-based lumped-parameter model is its simplicity, as it leads to a set of manageable equations. When the number of cells is sufficiently large, this model approximates the heat exchanger's actual behaviour well. Moreover, it offers flexibility for modelling different flow configurations within a specific exchanger design.

The equations governing the condenser's dynamic behaviour are derived based on the energy balance within a defined control volume, as illustrated in Fig. 7a. The control volume encompasses the entire condenser, modelled as a lumped parameter system. The energy accumulation within this control volume is determined by subtracting the energy leaving the system through the outflowing fluid and heat transfer from the energy entering in the inflowing fluid. Heat transfer can occur into or out of the control volume via convection. This energy balance is mathematically expressed through three ordinary differential equations (assuming in the condenser $T_{Csi}=T_{Cso}$), (12), (13), and (14), which account for the energy exchanges in the tube-side fluid, the tube walls, and the shell-side fluid, respectively [36].

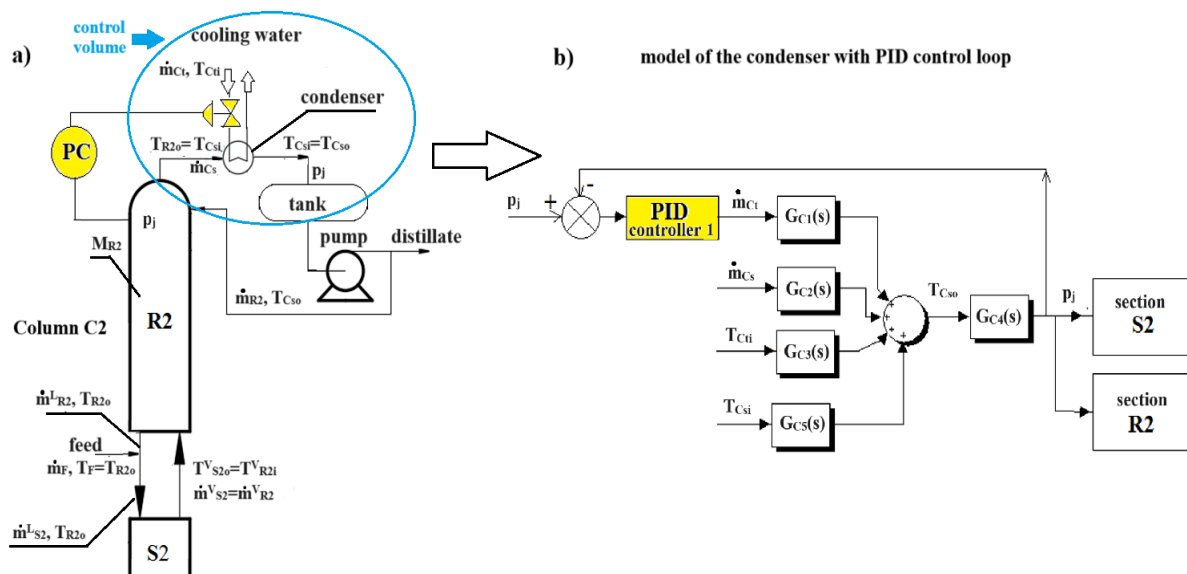


Figure 7. The scheme of distillation column C2 – a), and the block diagram for the dynamic model of the condenser with pressure PID controller – b).

$$\frac{dT_{Cto}}{dt} = a_{C1} \cdot \dot{m}_{Ct} \cdot (T_{Cti} - T_{Cto}) + a_{C2} \cdot (T_{Cm} - T_{Cto}) \quad (12)$$

$$\frac{dT_{Cm}}{dt} = a_{C3} \cdot (T_{Cto} - T_{Cm}) + a_{C4} \cdot (T_{Cso} - T_{Cm}) \quad (13)$$

$$\frac{dT_{Cso}}{dt} = a_{C5} \cdot \dot{m}_{Cs} + a_{C6} \cdot (T_{Cm} - T_{Cso}) \quad (14)$$

where constants a_{C1} - a_{C6} are defined as follows:

$$a_{C1} = \frac{1}{\rho_{Ct} \cdot V_{Ct}}, \quad a_{C2} = \frac{n_C \cdot \pi \cdot d_{C1} \cdot l_C \cdot h_{Ctz}}{\rho_{Ct} \cdot c_{Ct} \cdot V_{Ct}}, \quad a_{C3} = \frac{n_C \cdot \pi \cdot d_{C1} \cdot l_C \cdot h_{Ctz}}{\rho_{Cm} \cdot c_{Cm} \cdot V_{Cm}},$$

$$a_{C4} = \frac{n_C \cdot \pi \cdot d_{C2} \cdot l_C \cdot h_{CSz}}{\rho_{Cm} \cdot c_{Cm} \cdot V_{Cm}}, \quad a_{C5} = \frac{r_{Cs}}{\rho_{Cs} \cdot c_{Cs} \cdot V_{Cs}}, \quad a_{C6} = \frac{n_C \cdot \pi \cdot d_{C2} \cdot l_C \cdot h_{CSz}}{\rho_{Cs} \cdot c_{Cs} \cdot V_{Cs}},$$

The fouling effect on heat transfer within the condenser is accounted for because the formulas to calculate heat transfer coefficients incorporate the thermal resistances contributed by fouling layers on both the tube-side and shell-side:

$$h_{Ctz} = \frac{h_{Ct}}{h_{Ct} \cdot R_{fCt} + 1}, \quad h_{CSz} = \frac{h_{Cs}}{h_{Cs} \cdot R_{fCs} + 1} \quad (15), (16)$$

The mathematical model for the condenser, governed by equations (12)–(14), enables the determination of relationships using operator transmittances. These relationships link disturbances at the model's inlet with resulting temperature changes at the outlet, as illustrated in Fig. 7b. The initial interactions associated with energy exchange, represented by the transmittances G_{C1} , G_{C2} , G_{C3} and G_{C5} , were analysed. Additionally, the model includes the pressure effect on the condenser's dynamic behaviour, described by the transmittance G_{C4} .

The dynamic behaviour of the reboiler is described using equations derived from the energy balance within a designated control volume, as illustrated in Fig. 8a.

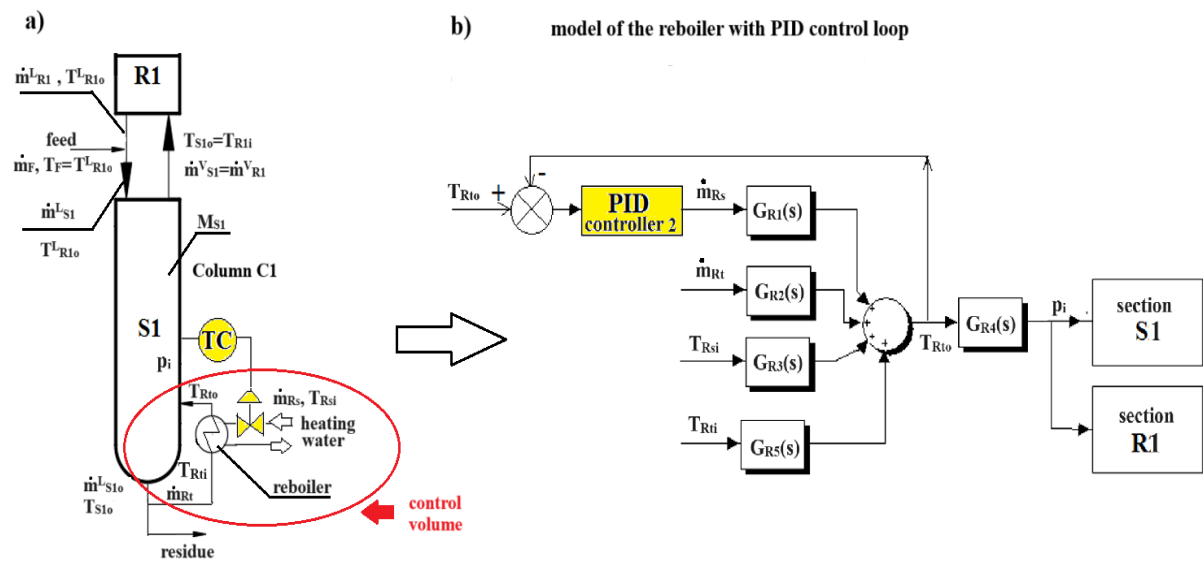


Figure 8. The scheme of distillation column C1 – a), and the block diagram for the dynamic model of the reboiler with temperature PID controller – b).

In this model, the control volume represents the entire reboiler, treated as a lumped parameter system. The energy accumulated in this volume is determined by subtracting the energy leaving through the outflowing fluid and the heat transferred out by convection (or adding heat transferred in) from the energy entering with the inflowing fluid. This energy balance is mathematically formulated using three ordinary differential Eqs. (17)-(19). These equations (assuming in the reboiler $T_{Rti}=T_{Rto}$) specifically address the energy balances for the tube-side fluid, the tube walls, and the shell-side fluid, respectively [36].

$$\frac{dT_{Rto}}{dt} = a_{R1} \cdot \dot{m}_{Rt} + a_{R2} \cdot (T_{Rm} - T_{Rto}) \quad (17)$$

$$\frac{dT_{Rm}}{dt} = a_{R3} \cdot (T_{Rto} - T_{Rm}) + a_{R4} \cdot (T_{Rso} - T_{Rm}) \quad (18)$$

$$\frac{dT_{Rso}}{dt} = a_{R5} \cdot \dot{m}_{Rs} \cdot (T_{Rsi} - T_{Rso}) + a_{R6} \cdot (T_{Rm} - T_{Rso}) \quad (19)$$

where constants a_{R1} - a_{R6} are defined as follows:

$$a_{R1} = -\frac{r_{Rt}}{\rho_{Rt} \cdot c_{Rt} \cdot V_{Rt} \cdot (1 - \alpha_{Rt})}, \quad a_{R2} = \frac{n_R \cdot \pi \cdot d_{R1} \cdot l_R \cdot h_{Rtz}}{\rho_{Rt} \cdot c_{Rt} \cdot V_{Rt} \cdot (1 - \alpha_{Rt})}, \quad a_{R3} = \frac{n_R \cdot \pi \cdot d_{R1} \cdot l_R \cdot h_{Rtz}}{\rho_{Rm} \cdot c_{Rm} \cdot V_{Rm}},$$

$$a_{R4} = \frac{n_R \cdot \pi \cdot d_{R2} \cdot l_R \cdot h_{RSZ}}{\rho_{Rm} \cdot c_{Rm} \cdot V_{Rm}}, \quad a_{R5} = \frac{1}{\rho_{Rs} \cdot V_{Rs}}, \quad a_{R6} = \frac{n_R \cdot \pi \cdot d_{R2} \cdot l_R \cdot h_{RSZ}}{\rho_{Rs} \cdot c_{Rs} \cdot V_{Rs}},$$

Heat transfer coefficients accounting for the fouling effect on heat transfer in the reboiler are calculated using equations that incorporate the thermal resistances of fouling layers on both the tube-side and shell-side, according to Eqs. (20) and (21). These resistances significantly affect the overall efficiency of heat exchange.

$$h_{Rtz} = \frac{h_{Rt}}{h_{Rt} \cdot R_{fRt} + 1}, \quad h_{RSZ} = \frac{h_{Rs}}{h_{Rs} \cdot R_{fRs} + 1} \quad (20), (21)$$

Relationships involving operator transmittances are established by solving Eqs. (17)-(19) in the reboiler's mathematical model, linking inlet disturbances to temperature variations at the outlet, as illustrated in Fig. 8b. The initial interactions concerning energy transfer, represented by the transmittances G_{R1} , G_{R2} , G_{R3} and G_{R5} , were determined. Additionally, the model incorporates the effects of pressure on the reboiler's dynamic response, captured through the transmittance G_{R4} .

3. Case study – results and discussion

The repositories [39] and [40] contain research material corresponding to the simulation results discussed in section 3, which validate the case study's findings. It also includes code, models, algorithms, and other valuable information associated with the project. A comprehensive block diagram of the HHIDiS system, illustrating the interdependencies between model components, should be made before building the computer-aided dynamic model. The entire block structure of the HHIDiS system is quite complex since it is thought of as a group of various process equipment pieces connected, as depicted in Fig. 2. It is possible to construct and turn the HHIDiS system block diagram, shown in Fig. 9, into a tool for simulation by using the Simulink application in a MATLAB platform. The authors focused only on modelling heat and mass transfer inside the devices. According to the authors, the main sources of dynamics are areas of intense heat and mass transfer inside the devices. On the other hand, in industrial applications,

engineers use short pipes connecting devices, and heat transfer is not intensive because heat is transferred to the environment through insulation. As a result, the calculations do not take into account additional delay times due to piping connecting different equipment. This approach is used by the vast majority of researchers, and the impact of such assumptions on the overall analysis in terms of the predictive capability of the model and PID control is negligibly small. Establishing a database with the steady-state values of the operating parameters in each process equipment unit is required. The current study has accomplished this by computing thermal-flow parameters. To be more precise, the database contains the following information for every apparatus: mass/molar flows, heat transfer coefficients, the thermal resistance of fouling, geometrical parameters, and thermophysical parameters of the fluids, such as densities, heat capacities, dynamic viscosities, and thermal conductivities, etc.

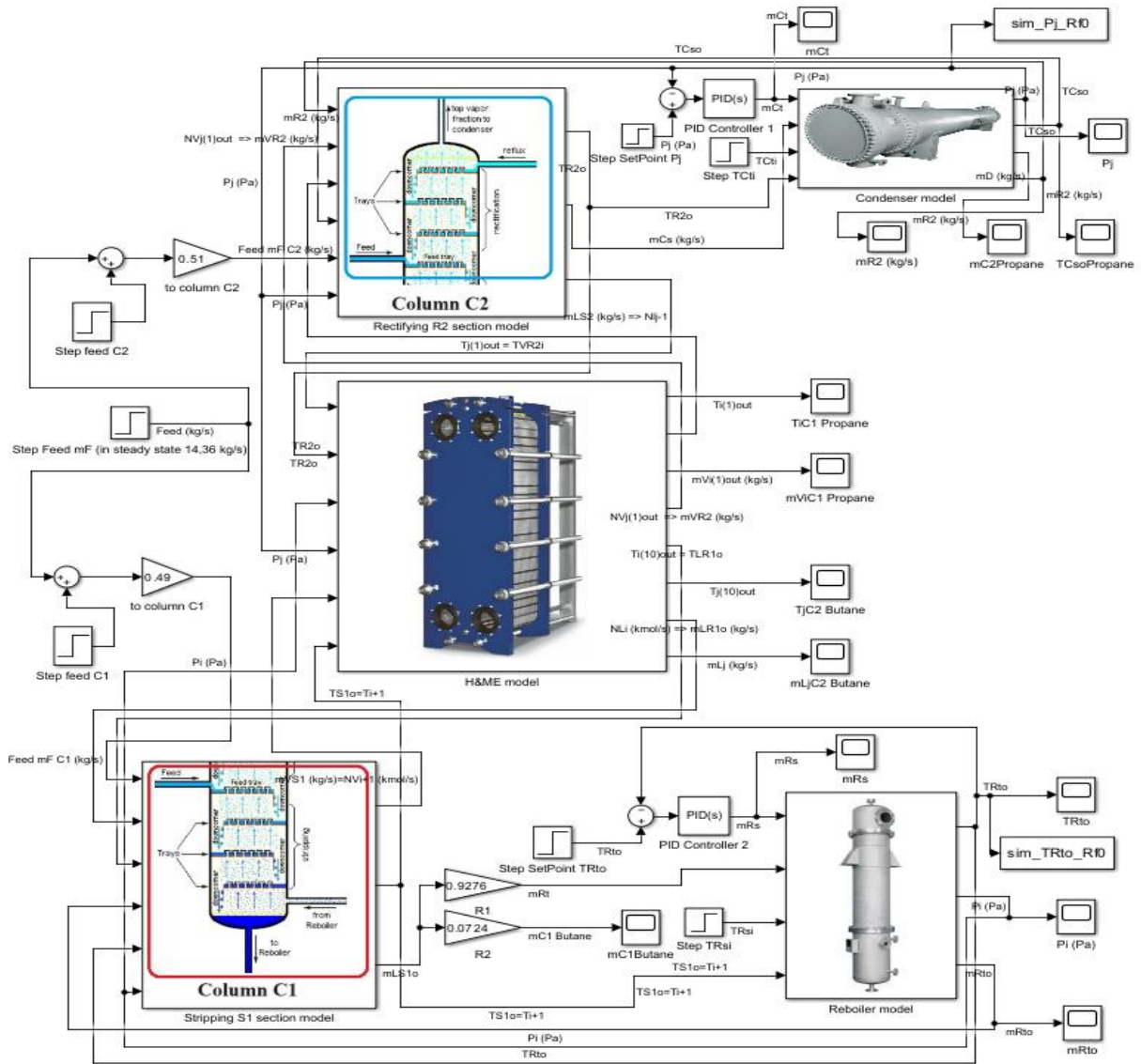


Figure 9. A view of the developed Simulink block diagram of the HHIDiS system in accordance with the Fig. 2.

3.1. Thermal-flow calculations for HHIDiS in steady state

The steady-state mathematical model proposed by Markowski et al. [5] was used to determine thermal-flow calculations and the selection of geometric parameters for HME. The process flow diagram in Fig. 2 was considered, where the calculated HME consists of rectifying R1 and

stripping S2 sections. However, calculations for the classic distillation of the S1 stripping section of the C1 column and the R2 rectification section of the C2 column were carried out using the AspenHysys V11 software. The following data were assumed, according to work [33]. The feed of the HHIDiS (Figs. 2 and 9) is a mixture of propane and butane with a 0.45-mole fraction of propane. The molar flowrates of feed for the C1 and C2 columns are 490 kmol/h and 510 kmol/h, respectively. Hence, in the schematic of the developed Simulink model including feedback PID controllers (Fig. 9), there are gain blocks with molar ratio values of 0.49 and 0.51 to ensure proper feed distribution to columns C1 and C2. Similarly, in Fig. 9, there are gain blocks with values of mass ratios: 0.9276 of butane, returned through the reboiler and fed as vapour to column C1, and 0.0724 of butane in residue discharged from column C1 as product. The mole fractions of propane in residue and distillate are 0.01 and 0.99, respectively. The temperature of the cooling water in the condenser at the inlet/outlet is 20/25°C, and the heating water temperature in the reboiler is 160/150°C. The pressures in the C1 and C2 distillation columns are 2500 kPa and 1000 kPa, respectively.

The number of theoretical mixing zones in plate HME, equivalent to theoretical trays, and the column profiles were determined using model equations by Markowski et al. [5]. The calculation resulted in 100 theoretical mixing zones. Considering a tray efficiency of 0.6, the actual number of mixing zones was calculated to be 167. The column profiles, adapted from reference [33], are symbolically depicted in Fig. 3b. Furthermore, a minimum temperature difference of 3 K was assumed between the column profiles (sections R1 and S2) in the temperature-enthalpy (T-H) diagram. The geometrical parameters of HME were calculated, and the channel geometry (Z-type channel as in work [35]) and the apparatus dimensions are the following [33]. The heat transfer area is 918 m² (248 plates), the plate size is 1.8 m x 2.05 m (3.7 m² per plate), and the clearance between plates is 10 mm, as shown in Fig. 10.

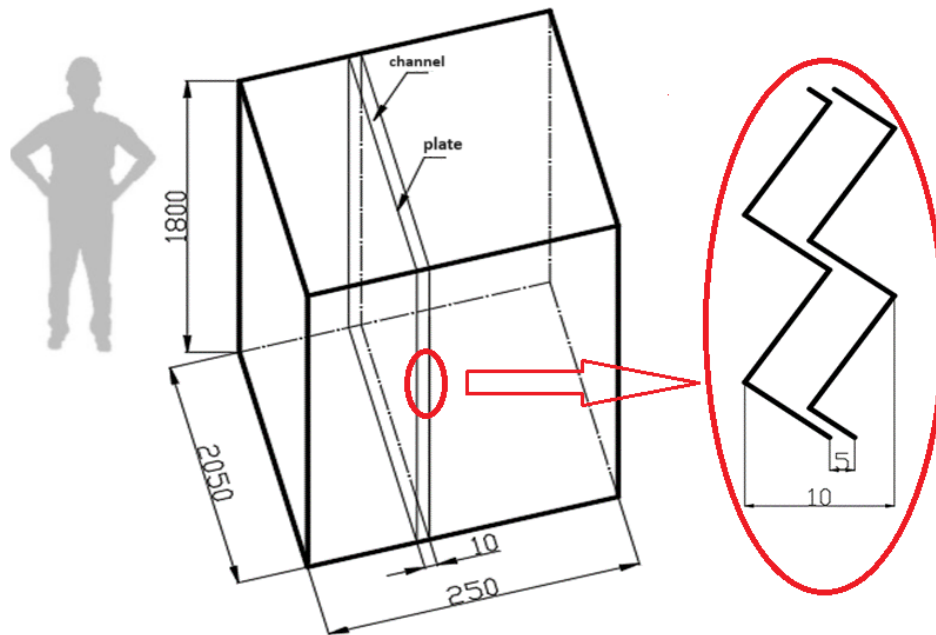


Figure 10. The assumed geometry of the apparatus frame (on the left) with Z-type channel geometry details (on the right).

Then, thermal-flow calculations for the reboiler of the C1 column and the condenser of the C2 column (see Fig. 2) were carried out using the HTRI Xchanger Suite 7.3.2 software. The obtained results are presented in Figs. 11 and 12.

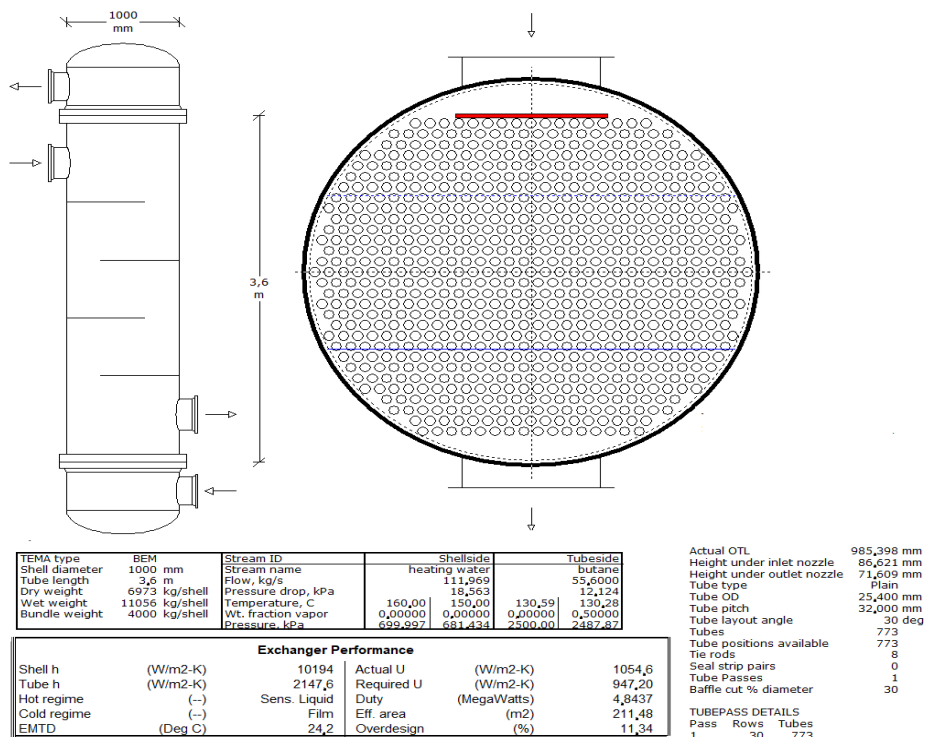


Figure 11. The assumed operational parameters and geometry details of the reboiler coupled with column C1.

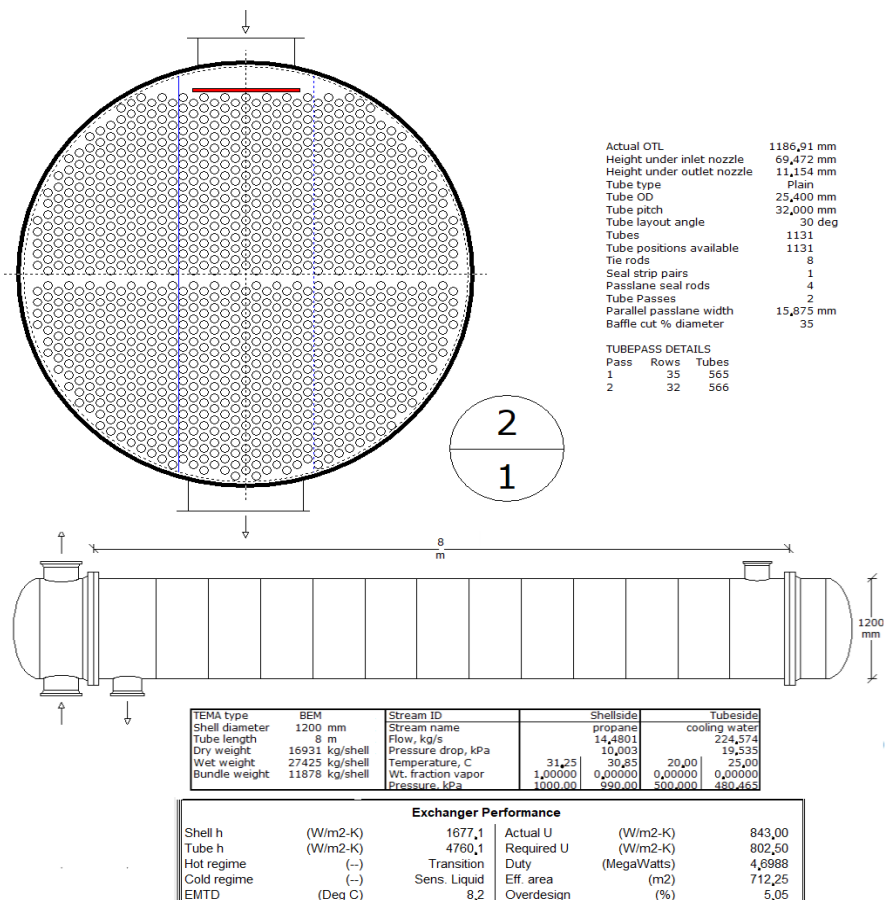


Figure 12. The assumed operational parameters and geometry details of the condenser coupled with column C2.

3.2. Study on the influence of industrial constraints on the PID-controlled HHIDiS

Studying the open-loop HME model step responses simulated with varying industrial restrictions, such as fouling build-up (R_f parameter) for all exchangers (HME, reboiler, and condenser), and with varying liquid hold up (β parameter) in the HME exchanger Z-type channels, is the first step. A number of open-loop simulations were performed in the Simulink/Matlab platform using only the created dynamic model of HME without the rest of the apparatus of the HHIDiS and without PID control loops (only the block diagram in Fig. 4). Changes in the exchanger's dynamic behaviours result from changes in its thermal inertia caused by increases in the parameters R_f or β , according to work [33]. Fig. 13a shows a typical thermal system's open-loop response and its standard indications describing dynamic features: gain K_o , delay time t_d and time constant t_l .

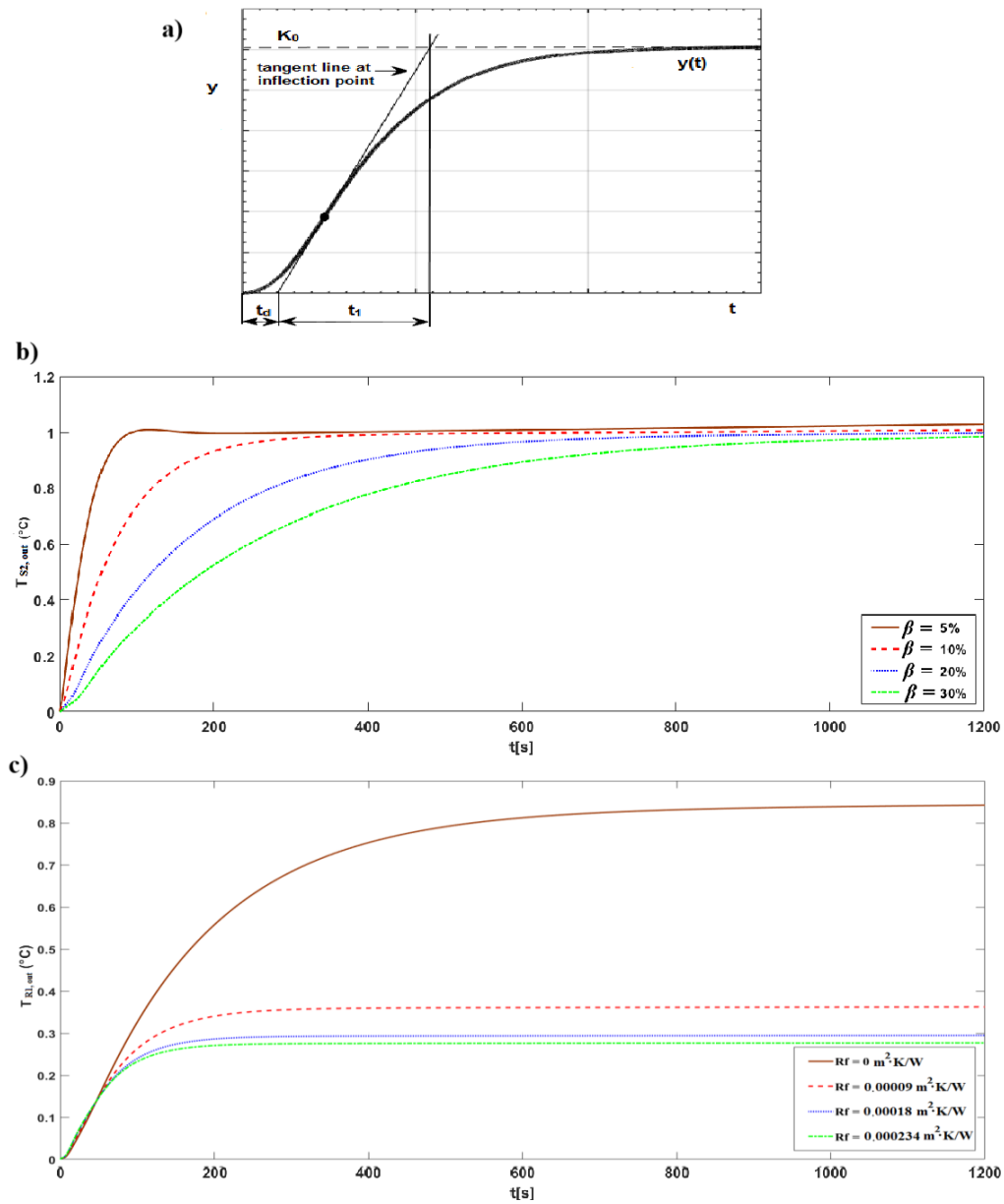


Figure 13. An open-loop unit step response of a typical thermal system a), the step responses of a plate HME for the assumed values of β parameter [33] - b) and the step responses of a plate HME for the assumed values of R_f parameter [33] - c).

For the predicted hold up of liquid β (5%, 10%, 20%, and 30%) in the HME channels, the open-loop residue temperature responses $T_{S2,out}$ of the HME model are displayed for a step change of +5% in the flowrate $\dot{N}_{R1,in}^V$ in Fig. 13b. A step change of +5% in the molar flowrate $\dot{N}_{R1,in}^V$ of vapours moving from the stripping S1 section to the rectifying R1 section, for the specified R_f parameter, is displayed against the open-loop distillate temperature responses $T_{R1,out}$ of the HME model in Fig. 13c. As can be seen in these sample responses (for evaluation of more characteristics, please refer to work [33]), the values of gain K_o , delay time t_d and time constant t_l vary following changes in parameter R_f or β . These characteristics from Fig. 13b demonstrate that all outlet signals approach an asymptotic value after around 1000 seconds. Furthermore, as shown by varying steps response parameters (gain, time constant, and delay time) in Tab. 1, the impact of the parameter β on characteristics course is visible.

Table 1. The dynamic features for step responses according to Fig. 13b.

The parameter β [%]	Gain – K_o [K · s/kmol]	Time constant - t_l [s]	Delay time - t_d [s]
5%	55,870	34.2	1.7
10%	54,780	105.3	3.1
20%	54,130	208.2	9.4
30%	53,420	307.3	15.5

The asymptotic open-loop responses of outlet signals to step changes in input signals are shown in Fig. 13b. The same scenario applies to any other randomly chosen inlet-outlet signal interaction documented in the authors' previous work [33]. The tested HME is, hence, dynamically stable. The dynamic stability of HME is supported by the range of changes in the values of the parameters, such as gain, time constant, and delay time (see Tab. 1), with respect to the liquid hold up - β in the HME channels. This is applicable even though the characteristics reach different values of these parameters.

The open-loop characteristics that are displayed in Fig. 13c demonstrate how fouling resistance affects outlet signals. After around 800 seconds, all outlet signals approach the asymptotic value, according to Fig. 13c. From the perspective of a process control system, fouling resistance also has a considerable impact on the characteristics course. It may be verified by examining the information in Tab. 2. When the fouling resistance value varies, the dynamic parameters (gain, time constant and delay time) also fluctuate greatly.

Table 2. The dynamic features for step responses according to Fig. 13c.

The parameter R_f [m ² K/W]	Gain – K_o [K · s/kmol]	Time constant - t_l [s]	Delay time - t_d [s]
0	45,490	250.7	10
0.00009	19,490	111.7	7
0.00018	15,970	91.3	5
0.000234	15,000	87	4

Fouling significantly influences the course of characteristics, as evidenced by Fig. 13c and the open-loop responses documented in the authors' previous work [33]. It can be quantitatively demonstrated by looking into the information in Tab. 2. While the delay time values are

essentially unchanged from the perspective of industrial applications, the values of dynamic factors like gain and time constant change notably in this case. To attain the requisite distillate purity, it is crucial to consider the impact of fouling during the HME exchanger's design phase by appropriately over-dimensioning the heat exchange surface.

In summary, the simulation findings in the authors' previous work [33] and reported in the repository [39], as well as the representative results in Fig. 13, demonstrate that plate HME is resistant to industrial limitations. One can envisage the application of such technology in any industry. Nevertheless, the HME is susceptible to extremely high fouling, which is brought on by its channel-type exchanger design (Fig. 10).

The observed variations in the gain, delay time, and time constant values in the examined open-loop step responses may significantly degrade the quality of PID control due to fouling accumulation on the exchangers' heat transfer surfaces and shifting liquid hold up in the HME. Investigating the three tuning components of each PID controller (the gains: K_p , K_i and K_d), as well as examining the ensuing transient responses (closed-loop characteristics), are recommended to avoid that.

Fig. 9 represents the process control system for the HHIDiS, including feedback PID controllers (pressure PID controller 1 for condenser - Fig. 7b and temperature PID controller 2 for reboiler, see Fig. 8b), which has been modelled and implemented in the Simulink/Matlab R2023b software. The gain values in the proportional, integral and derivative components of PID controllers usually can be derived using the Ziegler and Nichols approach [41], but in this study were determined using automatic PID tuning in Simulink (*PID Tuner App*) aimed at saving development time by providing a good initial set of control parameters for HHIDiS system and ensuring correct system operation. For both of the studied control loops, PID controllers 1 and 2 were separately tuned, and the recommended values of gains K_p , K_i , and K_d are presented in Tab. 3. From the control viewpoint, the pressure in the condenser (P_j) and temperature in the reboiler (T_{Rto}) are controlled variables. The associated manipulated variables are the mass flowrate of cooling water in the condenser (m_{Ct}) and the mass flowrate of heating water in the reboiler (m_{Rs}) – see Fig. 9. Two main tasks were investigated for each controlled variable: the reference tracking and the regulatory problems.

Table 3. The gain values in the PID components.

Tuning parameters	PID controller 1 of condenser	PID controller 2 of reboiler
K_p	-0.0095	1.80
K_i	-0.00053	0.97
K_d	0	0

Studies of the HHIDiS control system's transient responses are required to assess any potential negative impacts of parameters R_f and β on the control quality. Usually, evaluating the linear control systems' closed-loop characteristics includes analysing the responses to a unit input signal $1(t)$. An example response of a heat exchanger's temperature control system (a linear system of second order) is shown in Fig. 14.

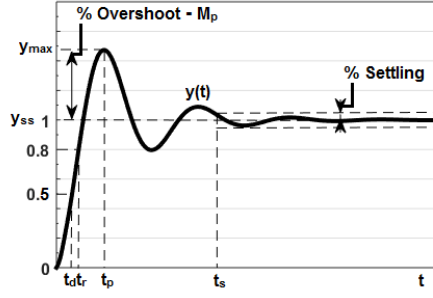


Figure 14. A typical closed-loop step response of a heat exchanger's control system (second-order linear system).

The indices specified below can be used to describe and assess the control quality for particular dynamic features that are comparable to those depicted in Fig. 14.

- Overshoot M_p is the percentage of the step response's $y(t)$ highest deviation from its steady-state value:

$$M_p = ((y_{max} - y_{ss}) / y_{ss}) \cdot 100\% \quad (39)$$

where: y_{ss} denotes $y(t)$ value at steady state ($y_{ss} \leq y_{max}$), and $y_{max} - y(t)$ value at its maximum. Large overshoot levels are not advised; the overshoot value is established during control-system design and can be used as an indicator of system stability.

- The peak time t_p is the time span that step response requires to reach its maximum ($y(t_p) = y_{max}$).
- The delay time t_d is the time required for $y(t)$ to reach 50% of its value at steady state ($y(t_d) = 0.5 y_{ss}$).
- The rise time t_r is the span of time after which the step response reaches 80% of its steady state value ($y(t_r) = 0.8 y_{ss}$).
- Finally, the settling time t_s is the time required for $y(t)$ to settle close to its steady-state with the tolerance margin, typically: $y_{ss} \pm 5\%$ (Fig. 14).

The mentioned quality indices are simple to calculate and may be used to assess the control system's features (closed-loop characteristics with varying values of R_f and β) based on how it reacts to step changes in variables associated with the process.

Based on values suggested by tubular exchanger manufacturers association (TEMA) standards [42], the authors hypothesised the R_f values of the plate HME, condenser and reboiler that were employed in the simulation studies (according to Tab. 4).

Table 4. Values of the R_f parameter according to TEMA standards.

Exchanger	Fouling parameter $R_f \cdot 10^{-4} \text{ (m}^2\text{K/W)}$			
	R_{f0} clean	R_{f1} low fouling	R_{f2} medium fouling	R_{f3} high fouling
HME exchanger				
R1 section "i" – propane/butane mixture	0	0.9	1.8	2.34
S2 section "j" – propane/butane mixture	0	0.9	1.8	2.34
Condenser				
shell side – propane	0	0.9	1.8	2.34
tube side – cooling water	0	0.9	2.5	4.5
Reboiler				
shell side – butane	0	0.9	1.8	2.34
tube side – heating water	0	0.9	1.8	2.34

Based on simulated step responses of the HHIDiS models under study, with different R_f values corresponding to the heat-transfer surface clean or fouled, the closed-loop characteristics for PID controllers 1 and 2 are shown in Figs. 15 and 16, respectively. The PID tuning parameter values are assumed to align with Table 3 data for clean exchangers.

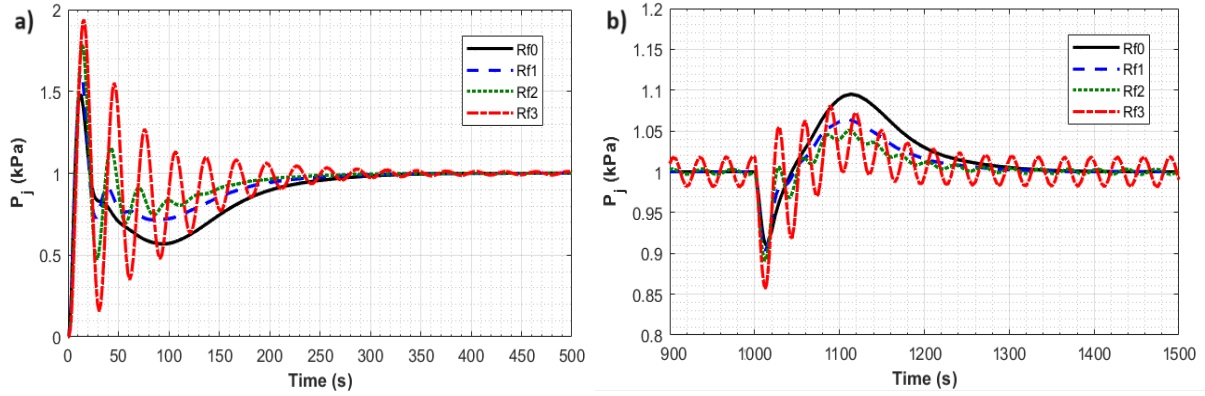


Figure 15. Closed-loop step responses of HHIDiS models with the different values of R_f parameter ensured by PID controller 1: set-point tracking a), disturbance rejection b).

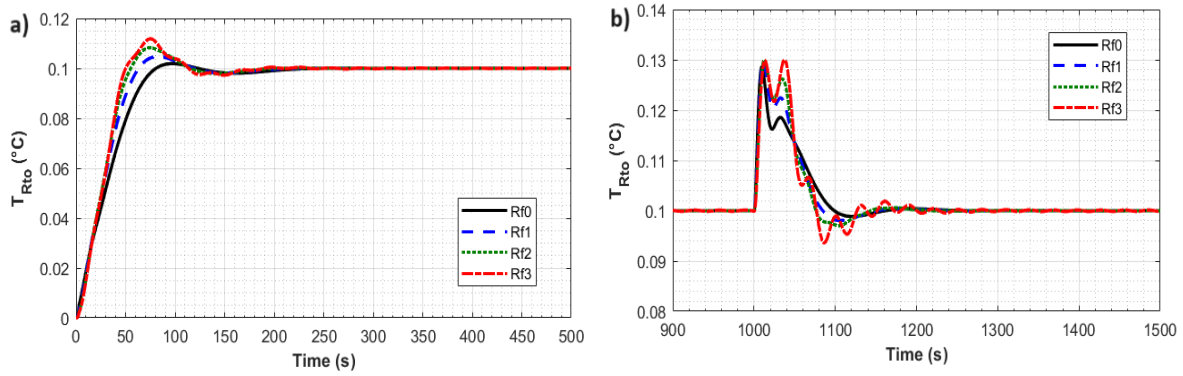


Figure 16. Closed-loop step responses of HHIDiS models with the different values of R_f parameter ensured by PID controller 2: set-point tracking a), disturbance rejection b).

The closed-loop step responses achieved for the clean and fouled heat-transfer surface with varying values of the R_f parameter (Figs. 15 and 16) demonstrate that fouling accumulation is followed by significant deterioration of control-quality indices. The overshoot, peak, delay, rise, and settling times change, as shown in Tab. 5.

Table 5. Control-quality indices for PID 1 and PID 2 controllers in relation to R_f parameter values.

Closed-loop responses	Parameter R_f	Control-quality indices				
		M_p (%)	t_p (s)	t_d (s)	t_r (s)	t_s (s)
PID controller 1 (Figure 15a)	R_{f0}	47.9	12.6	4.3	5.7	242
	R_{f1}	61.0	13	4.7	6.1	214
	R_{f2}	78.3	14.1	5.2	6.6	180
	R_{f3}	93.3	15.8	5.7	7.2	245
PID controller 2 (Figure 16a)	R_{f0}	1.9	96.5	29	50.7	212
	R_{f1}	4.7	82.1	26.1	43.5	195
	R_{f2}	8.3	75.5	25.9	39.4	184
	R_{f3}	11.9	75	25.4	38.6	185

The results of the simulations of transient responses for various values of the liquid hold up are displayed in Figs. 17 and 18. The graphs show that an increase in the β parameter in the HME exchanger causes negligible changes only in the control-quality indices for control loops 1 and 2. This result suggests that the liquid hold up would not negatively impact the control quality indices in the scenario under study, and therefore it is likely not necessary to modify the PID tuning settings (see Tab. 6).

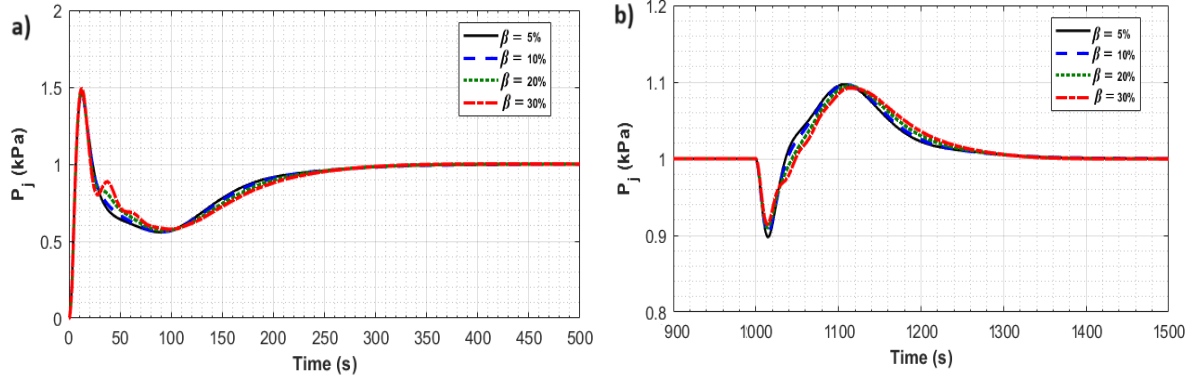


Figure 17. Closed-loop step responses of HHIDiS models with the different values of β parameter ensured by PID controller 1: set-point tracking a), disturbance rejection b).

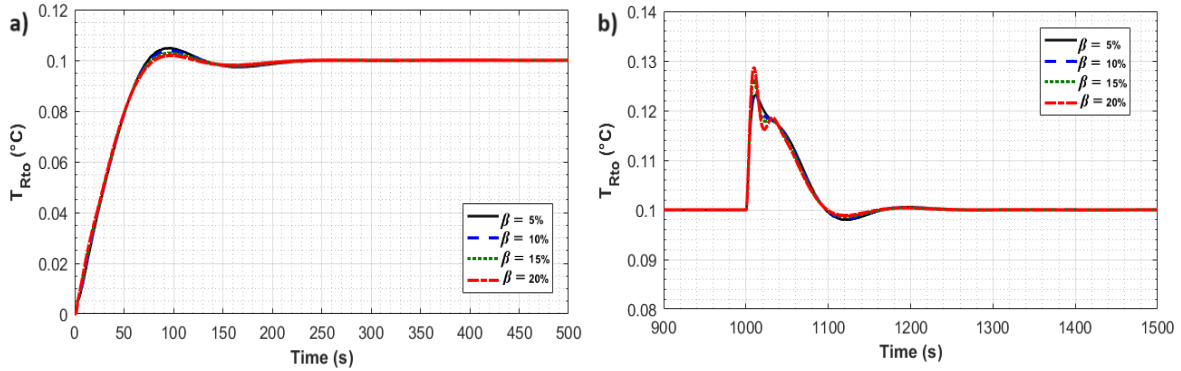


Figure 18. Closed-loop step responses of HHIDiS models with the different values of β parameter ensured by PID controller 2: set-point tracking a), disturbance rejection b).

Table 6. Control-quality indices for PID 1 and PID 2 controllers in relation to β parameter values.

Closed-loop responses	Parameter	Control-quality indices				
	β (%)	M_p (%)	t_p (s)	t_d (s)	t_r (s)	t_s (s)
PID controller 1 (Figure 17a)	5	45.7	12.5	4.2	5.6	236.8
	10	46.3	12.55	4.25	5.65	237.5
	20	47.9	12.6	4.3	5.7	242
	30	49.2	12.65	4.35	5.8	247.5
PID controller 2 (Figure 18a)	5	4.7	95	29.9	51.5	223
	10	3.8	96	29.6	51	221.2
	15	2.8	96.2	29.3	50.8	217.5
	20	1.9	96.5	29	50.7	212

3.3. Discussion

According to the open-loop trends of the HME, the suggested HHIDiS system (without compressor – Fig. 2) is stable, indicating that a standard PID controller may be used to regulate the process parameters. Other researchers have examined the steady-state and dynamic behaviour of the HIDiC and various PID control systems, such as for temperature [27], pressure [28], and top and bottom composition [43], as well as for a combination of these control variables [24]. The authors' simulation results are consistent with these findings. Research by Gutiérrez-Guerra et al. [18] explored controlling HIDiC columns with compressors and conventional designs, using both open-loop and closed-loop analyses. Proportional Integral (PI) controllers were chosen for their simplicity and reliability in managing industrial systems. Later, Gutiérrez-Guerra and Segovia-Hernández [32] modelled closed-loop operations with reference tracking and regulatory problems, leveraging detailed hydraulic simulations in Aspen Dynamics. Their findings emphasised that feed composition is vital for enhancing the efficiency of compressor-driven HIDiC setups.

This study revealed that increases in fouling resistance and liquid hold up significantly impact the thermal inertia of the HHIDiS system, altering its dynamic behavior. These changes were identified by analysing open-loop step responses of the HME dynamic model at various stages of fouling and liquid accumulation. The effects of fouling on heat exchanger surfaces and liquid hold up are reflected in the gain (K_o), delay time (t_d), and time constant (t_o), as shown in Tables 1 and 2. While delay time changes were minimal in most open-loop step responses, shifts in time constants and gain values could negatively affect PID control performance. Similar outcomes have been noted in PID-regulated shell-and-tube heat exchangers and their networks, as reported by the authors in [36]. A thorough assessment of PID tuning components and evaluation of closed-loop control quality are recommended to mitigate these issues.

In this study, the closed-loop step responses and control-quality indices, such as overshoot, peak time, delay time, rise time, and settling time were extensively investigated for controlled variables: the pressure in the condenser (P_j – in PID control loop 1) and temperature in the reboiler (T_{Rto} – in PID control loop 2) while taking into account the set-point tracking and disturbance rejection under industrial constraints - variable values of parameters R_f and β . Summarising the obtained results, the closed-loops simulations in this study show that the R_f parameter significantly affects the quality of PID control performance – see Tab. 5 and Figs. 15 and 16. However, considering the β parameter, despite its noticeable impact on the open-loop characteristics, this phenomenon did not cause a noticeable deterioration in the PID control-quality indices (Tab. 6) reported in the closed-loop characteristics in Figs. 17 and 18. Nevertheless, by periodically adjusting the optimal levels of PID gains, for instance, one can avoid adverse changes in control quality [44]. Thus, future research is required on the suggested HHIDiS technology with enhanced control loops (MPC) in an industrial setting. A more sophisticated method that Oravec [45] developed in collaboration with Markowski and Trafczynski would be appropriate to note in this context. Robust MPC with integrated action was employed in their cooperative efforts to optimise control performance when fouling influenced shell-and-tube heat exchanger dynamic operation, causing variations in the exchangers' characteristics.

4. Conclusions

- Numerical simulations indicate that the tested HME demonstrates robustness within a restricted range of typical signal fluctuations and industrial constraints, such as fouling formation and liquid hold up. This makes the HHIDiS model suitable for designing control systems for channel-type exchangers used in diaphragm heat exchange and thermal separation.

- Due to its channel or plate-based structure, the operation of the HME in the HHIDiS system is susceptible to intense fouling.
- The increase in the β parameter in the HME exchanger results in only marginal variations in control performance indices, specifically a slight increase in overshoot M_p from 45.7% to 49.2% for PID loop 1 and a decrease from 4.7% to 1.9% for PID loop 2. These changes suggest that the influence of liquid hold-up on control quality is negligible under the conditions studied, and thus, adjustment of the existing PID tuning parameters appears unnecessary.
- The results indicate that fouling, represented by increasing values of the R_f parameter, leads to a substantial degradation of control performance, with overshoot M_p in PID loops 1 and 2 increasing from 47.9% to 93.3%, and from 1.9% to 11.9%, respectively, among other notable changes in control-quality indices. These findings underscore the critical impact of heat-transfer surface fouling on dynamic behavior and control effectiveness.
- The closed-loop response analysis confirms the stability of HHIDiS technology under input signal variations and industrial limitations, supporting the use of standard PID controllers for automated process parameter management.
- Findings reveal that a substantial increase in fouling resistance without adjusting PID tuning parameters could result in temperature or pressure oscillations, slow set-point responses, and dangerous overshoots during the startup of the HHIDiS. Proper tuning of PID parameters can prevent such issues, with optimal values determined using dynamic modelling and validated through simulations.
- These insights contribute to advancing the control strategies for heat-integrated distillation systems by demonstrating that even under industrial disturbances like fouling and liquid hold-up, stable and efficient operation can be maintained with properly tuned PID controllers—thereby providing a practical framework for controller design in next-generation energy-efficient separation processes.
- By bridging dynamic modelling with control performance analysis under realistic operating challenges, this study establishes a foundational methodology for designing resilient control architectures in compact, high-efficiency HHIDiS, marking a step forward in the automation of sustainable chemical processing technologies.
- Future research will explore integrating robust control strategies, such as Model Predictive Control (MPC), into HHIDiS technology to enhance performance under varying industrial conditions. Achieving this requires a comprehensive energy efficiency, cost-effectiveness, and system dynamics analysis.

Nomenclature

Symbols

A : heat transfer surface of HME, m^2

B : molar heat of vaporisation (condensation), kJ/kmol

c : mass or molar specific heat, $\text{kJ}/(\text{kg}\cdot\text{K})$ or $\text{kJ}/(\text{kmol}\cdot\text{K})$

d_{C1}, d_{C2} : internal and external tube diameter of condenser, m

d_{R1}, d_{R2} : internal and external tube diameter of reboiler, m

dA : differential of the area of HME, m^2

$d\dot{Q}$: differential of the heat duty of HME, W

dt : differential of time, s

$G(s)$: operator transmittance

h_b : convective boiling heat transfer coefficient, $\text{W}/(\text{m}^2\cdot\text{K})$

h_c : condensation heat transfer coefficient, $\text{W}/(\text{m}^2\cdot\text{K})$

h_L : heat transfer coefficient for liquid, $\text{W}/(\text{m}^2\cdot\text{K})$

h^L, h^V : molar enthalpy of liquid and molar enthalpy of vapour, kJ/kmol
 K_d, K_i, K_p : derivative, integral and proportional gain
 K_o : gain, K·s/kmol
 l_C, l_R : length of the condenser and reboiler tubes, m
 m_{Ct} : mass flowrate of cooling water in condenser, kg/s
 m_{Rs} : mass flowrate of heating water in reboiler, kg/s
 \dot{m} : mass flowrate, kg/s
 M_p : overshoot, %
 M_{R2} : mas of liquid in the rectifying section R2 in column C2, kg
 M_{S1} : mas of liquid in the stripping section S1 in column C1, kg
 n_C, n_R : total number of condenser and reboiler tubes
 N_i, N_j : number of moles in the cell on the rectifying and stripping side, mol
 \dot{N}^L, \dot{N}^V : molar flow rate of liquid and molar flow rate of vapour, kmol/h
 p_j : pressure in the condenser and in the stripping section, kPa
 p_i : pressure in the reboiler and in the rectifying section, kPa
 \dot{Q} : heat duty of HME, W
 \dot{Q}_C, \dot{Q}_R : heat duty of condenser and heat duty of reboiler, W
 r : heat of vaporization (condensation), kJ/kg
 R_f : thermal resistance of fouling, m²·K/W
 s : Laplace operator
 t : time, s
 t_I : time constant, s
 t_d : delay time, s
 t_p : peak time, s
 t_r : rise time, s
 t_s : settling time, s
 T : temperature, °C
 ΔT : temperature difference, K
 T^L, T^V : temperature of liquid and temperature of vapour, °C
 T_{Rto} : temperature in reboiler, °C
 U_f, U_{ij} : overall heat transfer coefficient in the fouled and clean HME, W/(m²·K)
 V : volume, m³
 V_m : wall volume for the cell i, j , m³
 $y(t)$: step response of output variable
 y_{ss} : steady state value of output variable
 y_{max} : maximal value of output variable

Superscripts
 L, V : liquid and vapour

Subscripts
 C, R : condenser and reboiler
 Cs, Rs : condenser and reboiler shell-side
 Csi, Cso : inlet and outlet to/from the condenser shell-side
 Ct, Rt : condenser and reboiler tube-side
 Cti, Cto : inlet and outlet to/from the condenser tube-side
 i, j : -th cell on the rectifying side and on the stripping side
 m : wall
 Rsi, Rso : inlet and outlet to/from the reboiler shell-side
 Rti, Rto : inlet and outlet to/from the reboiler tube-side

R1, R2: rectifying section R1 in column C1 and rectifying section R2 in column C2

R1i, R1o: inlet and outlet to/from the rectifying section R1 in column C1

R2i, R2o: inlet and outlet to/from the rectifying section R2 in column C2

s: steady state value

S1, S2: stripping section S1 in column C1 and stripping section S2 in column C2

S1i, S1o: inlet and outlet to/from the stripping section S1 in column C1

S2i, S2o: inlet and outlet to/from the stripping section S2 in column C2

z: including thermal resistance of the fouling layer

Greek letters

α_{Rt} : volume fraction of vapors in a two-phase mixture in the tube-side of the reboiler

β : hold up of liquid, %

π : number pi

ρ : density, kg/m³

Abbreviations

HIDiC: heat-integrated distillation column

HHIDiS: hybrid heat-integrated distillation system

HME: heat and mass exchanger

IAE: integral absolute error

MPC: model predictive control

PID: proportional-integral-derivative

RDWC: reactive dividing wall column

TEMA: tubular exchanger manufacturers association

VRC: vapour recompression

CRedit authorship contribution statement

Mariusz Markowski: conceptualization, methodology, funding acquisition, project administration, data curation, writing – review and editing, investigation. **Marian Trafczynski**: methodology, formal analysis, funding acquisition, project administration, software, data curation, writing – review and editing, writing – original draft, visualization, investigation. **Erika Pavlovičová**: validation, writing – review and editing, supervision. **Juraj Oravec**: validation, writing – review and editing, supervision. **Slawomir Alabrudzinski**: methodology, software, data curation, funding acquisition, project administration, investigation. **Piotr Kisielewski**: software, visualization, investigation. **Krzysztof Urbaniec**: writing – original draft, writing – review and editing. **Kacper Elwertowski**: visualization, investigation. **Damian Gostynski**: visualization, investigation.

Declaration of competing interest

The authors declare that they have no known competing financial interests or personal relationships that could have appeared to influence the work reported in this paper.

Acknowledgements

MT, MM and SA gratefully acknowledge the contribution of the National Science Centre, Poland, under the projects 2021/43/B/ST8/01036 and 2023/07/X/ST8/01079.

EP and JO gratefully acknowledge the contribution of the Scientific Grant Agency of the Slovak Republic under the grant 1/0297/22, the Slovak Research and Development Agency under the project APVV-20-0261, and the Research and Innovation Authority (VAIA) under the grant no. 09I01-03-V04-00024 (Slovak Research Excellence in Advanced Control for Smart Industries). This research is funded by the European Union's Horizon Europe under grant no. 101079342 (Fostering Opportunities Towards Slovak Excellence in Advanced Control for Smart Industries).

Data availability

Data will be made available on request.

References

1. Jana A. K., Heat integrated distillation operation, *Applied Energy*, 2010. 87(5), 1477–1494. doi:10.1016/j.apenergy.2009.10.014
2. Kiss, A.A. Distillation technology-still young and full of breakthrough opportunities. *J. Chem. Technol. Biot.* 2014, 89, 479–498. doi:10.1002/jctb.4262
3. Tan H, and Cong L. Modeling and Control Design for Distillation Columns Based on the Equilibrium Theory. *Processes*. 2023; 11(2):607. doi:10.3390/pr11020607
4. Cong L, Liu D, Ling H. Global Modeling of Heat-Integrated Distillation Column Based on Limited Local Measurements. *Processes* 2024. 12(3):484. <https://doi.org/10.3390/pr12030484>
5. Markowski M., Alabrudzinski S., Storczyk S., Heat and mass exchanger model for hybrid heat integrated distillation systems (HHIDiS), *Applied Thermal Engineering*, 2020, 174: 115249. doi:10.1016/j.applthermaleng.2020.115249
6. Fang J., Cheng X., Li Z., Li H., Li C., A review of internally heat integrated distillation column, *Chinese Journal of Chemical Engineering*, 2019, 27(6), 1272–1281, 2019. doi:10.1016/j.cjche.2018.08.021
7. Alabrudzinski S., Suchecki W., Markowski M., Trafczynski M., Energy expenditure in the Z-type plate heat and mass exchanger based on the concept of heat-integrated distillation column, *Applied Thermal Engineering*, 2024. 256:123975, doi:10.1016/j.applthermaleng.2024.123975
8. Tang W-T., Chein Ch-K., Ward J.D., A review of energy intensification strategies for distillation processes: Cyclic operation, stacking, heat pumps, side-streams, dividing walls and beyond. *Separation and Purification Technology*, 2025. 357A:130030. doi:10.1016/j.seppur.2024.130030
9. Harvindran, V. and Foo, D.C. Design of Internally Heat-Integrated Distillation Column (HIDiC), *Process Intensification and Integration for Sustainable Design*, 2021. 117–129. doi:10.1002/9783527818730.ch6
10. Kiss A.A. and Olujić Ž. A review on process intensification in internally heat-integrated distillation columns, *Chemical Engineering and Processing: Process Intensification*, 2014. 86, 125–144. doi:10.1016/j.cep.2014.10.017
11. Velázquez J.J.H., Durán F.M.Z., Díaz L.A.C., Ruiz J.C., Avila J.R.A., Hybrid two-step optimization of internally heat-integrated distillation columns. *Journal of the Taiwan Institute of Chemical Engineers*, 2022. 130:103967. doi: 10.1016/j.jtice.2021.06.061
12. Marin-Gallego M., Mizzi B., Rouzineau D., Gourdon C., Meyer M. Concentric Heat Integrated Distillation Column (HIDiC): a new specific packing design, characterization and pre-industrial pilot unit validation. *Chem. Eng. Processing - Process Intensification*, 2022. 171: 108643. doi:10.1016/j.cep.2021.108643
13. Kagioulis P., Ramesh R., van Goethem M., Saric M., van Delft Y.C. Heat-integrated distillation columns as a retrofit cannot bring energy savings to the ethylene plant, *Ind. Eng. Chem. Res.* 2021. 60(19):7342–7351. doi:10.1021/acs.iecr.1c00500
14. Harwardt A. and Marquardt W. Heat-integrated distillation columns: Vapor recompression or internal heat integration? *AIChE J.* 2012. 58(12):3740–3750. doi:10.1002/aic.13775
15. Shenvi A.A., Herron D.M., Agrawal R. Energy efficiency limitations of the conventional heat integrated distillation column (HIDiC) configuration for binary distillation, *Ind. Eng. Chem. Res.* 2011. 50(1):119–130. doi:10.1021/ie101698f
16. Eyvazi-Abhari N., Khalili-Garakani A., Kasiri N. Reaction/distillation matrix algorithm development to cover sequences containing reactive HIDiC: Validation in optimized process of dimethyl carbonate production, *Energy* 2023, 276:127493. doi:10.1016/j.energy.2023.127493

17. Gao X., Yang Y., Chen M., Cheng Q., Lu K. Study on a novel reactive internally heat integrated distillation process for the synthesis of ethyl acetate and its column configuration, *Sep. Purif. Technol.* 2022. 300:121755. doi:10.1016/j.seppur.2022.121755
18. Gutiérrez-Guerra, R., Segovia-Hernández, J. G., & Hernández, S. Study of dynamic performance of heat-integrated distillation columns considering the effect of relative volatility of the mixtures. *Chemical Engineering Research and Design*, 2023, 191:446-461 DOI: 10.1016/j.cherd.2023.01.032
19. Liu M., Gao W., Yan K., Li Y., Li B., Zhang J., Sun W., Zhao L. A separation column for liquid mixture based on phase transform: Experiment and simulation. *Chinese Journal of Chemical Engineering* 2024. 74:144-153. doi:10.1016/j.cjche.2024.06.010
20. Nakaiwa M., Huang K., Endo A., Ohmori T., Akiya T., Takamatsu T. Internally heat-integrated distillation columns: a review, *Chemical Engineering Research and Design*, 2003. 81(1):162–177. doi:10.1205/026387603321158320
21. Zhu, S.; Yang, A.; Kong, Z.Y.; Sun, S.; Bai, M.; Sunarso, J. Control of heat-integrated indirect triple-column extractive distillation for separating ternary azeotropic mixture tetrahydrofuran-ethyl acetate-water. *Sep. Purif. Technol.* 2023, 308:122951. doi:10.1016/j.seppur.2022.122951
22. Cong, L. and Liu, X. Nonlinear-Model-Based Control of a Heat Integrated Distillation Column Using Model Updating Based on Distributed Wave Velocity. *Ind. Eng. Chem. Res.* 2019, 58, 20758–20768. doi:10.1021/acs.iecr.9b04457
23. Luyben, W.L. Control of heat-integrated extractive distillation processes. *Comput. Chem. Eng.* 2018, 111:267–277. doi:10.1016/j.compchemeng.2017.12.008
24. Ho T. J., Huang C. T., Lin J. M., Lee L. S., Dynamic simulation for internally heat-integrated distillation columns (HIDiC) for propylene–propane system. *Computers & Chemical Engineering*, 2009. 33(6):1187-1201. doi:10.1016/j.compchemeng.2009.01.004
25. Seo C., Lee H., Lee M., Lee J. W., Temperature Driven Internal Heat Integration in an Energy-efficient Partial Double Annular Column. *Korean Journal of Chemical Engineering*, 2022. 39, 263–274. doi: 10.1007/s11814-021-0937-7
26. Huang K., Shan L., Zhu Q., Qian J., Design and control of an ideal heat-integrated distillation column (ideal HIDiC) system separating a close-boiling ternary mixture, *Energy*, 2007, 32(11):2148-2156. doi:10.1016/j.energy.2007.04.007
27. Huang K., Wang S. J., Iwakabe K., Shan L., Zhu Q., Temperature control of an ideal heat-integrated distillation column (HIDiC), *Chemical Engineering Science*, 2007. 62(22):6486-6491. doi:10.1016/j.ces.2007.05.015
28. Huang K., Matsuda K., Takamatsu T., Nakaiwa M., The Influences of Pressure Distribution on an Ideal Heat-Integrated Distillation Column (HIDiC), *Journal of Chemical Engineering of Japan*, 2006. 39(6):652-660. doi:10.1252/jcej.39.652
29. Jana A. K., An Internal Thermal Integration Arrangement for Multicomponent Batch Rectifier: Introducing Vapor Recompression Mechanism, *Chemical Engineering and Processing - Process Intensification*, 2022. 180:108771. doi: 10.1016/j.cep.2021.108771
30. Nakaiwa M., Huang K., Endo A., Naito K., Owa M., Akiya T., Nakane T., Evaluating Control Structures for a General Heat Integrated Distillation Column (General HIDiC), *Computers and Chemical* 1999, 23:S851-S854. doi:10.1016/S0098-1354(99)80209-9
31. Gutiérrez-Guerra, R., & Segovia-Hernández, J. G. Novel approach to design and optimize heat-integrated distillation columns using Aspen Plus and an optimization algorithm. *Chemical Engineering Research and Design*, 2023, 196:13-27. doi: 10.1016/j.cherd.2023.06.015
32. Gutiérrez-Guerra, R., & Segovia-Hernández, J. G. Impact of the control properties on the energetic and economic performance of Heat-Integrated Distillation Columns under variable feed composition. *IFAC Journal of Systems and Control*, 2024, 27: 100256. doi:10.1016/j.ifacsc.2024.100256

33. Markowski M., Trafczynski M., Kisielewski P., The dynamic model of a rectification heat exchanger using the concept of heat-integrated distillation column. *Energy*, 2022. 256:124622. doi:10.1016/j.energy.2022.124622
34. Varbanov, P. S., Klemeš, J. J., Friedler, F. Cell-based dynamic heat exchanger models—Direct determination of the cell number and size. *Computers & chemical engineering*, 2011, 35(5):943-948. doi:10.1016/j.compchemeng.2011.01.033
35. Alabrudzinski S., Suchecki W., Markowski M., Trafczynski M., Energy expenditure in the Z-type plate heat and mass exchanger based on the concept of heat-integrated distillation column, *Applied Thermal Engineering*, 2024, 256:123975. doi:10.1016/j.applthermaleng.2024.123975.
36. Trafczynski M., Markowski M., Alabrudziński S., Urbaniec K., The influence of fouling on the dynamic behavior of PID-controlled heat exchangers. *Applied Thermal Engineering*, 2016, 109:727–738. doi:10.1016/j.applthermaleng.2016.08.142
37. Carvalho CB, Carvalho EP, Ravagnani MASS. Dynamic analysis of fouling buildup in heat exchangers designed according to TEMA standards. *Ind Eng Chem Res* 2018, 57:3753–3764. doi:10.1021/acs.iecr.7b05306
38. Mathisen KW, Morari M, Skogestad S. Dynamic models heat exchangers and heat exchanger networks. *Comput Chem Eng* 1994, 18:S459–S463. doi:10.1016/0098-1354(94)80075-8
39. Trafczynski M., Markowski M., 2024, "Development of a dynamics model and simulation studies of dynamic characteristics of an integrated plate apparatus for thermal separation of substances with simultaneous diaphragm heat exchange, subject to industrial limitations.", <https://doi.org/10.18150/VMTWCD>, RepOD, V1
40. Trafczynski M., Markowski M., Pavlovičová E., Oravec J., 2024, "Development of a dynamics model and the study on the influence of industrial constraints on the dynamic behavior of a PID-controlled and robust MPC-controlled hybrid heat-integrated distillation system with heat and mass exchanger.", <https://doi.org/10.18150/IOVWN5>, RepOD, V1.
41. Ziegler, J. G., & Nichols, N. B. Optimum settings for automatic controllers. *Trans ASME*, 1942, 64(8):759-765. doi:10.1115/1.4019264
42. Tubular Exchanger Manufacturers Association. Standards of the Tubular Exchanger Manufacturers Association, 8th ed.; TEMA: New York, NY, USA, 1999.
43. Huang K., Nakaiwa M., Akiya T., Aso K., Takamasu T. A Numerical Consideration on Dynamic Modeling and Control of Ideal Heat-Integrated Distillation Columns, *Journal of Chemical Engineering of Japan*, 1996, 29(2):344-351. doi:10.1252/jcej.29.344
44. Trafczynski M., Kisielewski P., Markowski M., Urbaniec K., A modeling framework to investigate the influence of fouling on the dynamic characteristics of PID-controlled heat exchangers and their networks, *Applied Sciences*, 2019, 9(5):824. doi:10.3390/app9050824
45. Oravec J., Bakošová M., Trafczynski M., Vasičkaninová A., Mészáros A., Markowski M., Robust model predictive control and PID control of shell-and-tube heat exchangers. *Energy*, 2018, 159:1-10. doi:10.1016/j.energy.2018.06.106